Chemical and Biological Technologies in Agriculture

RESEARCH

Open Access

Green approach for the synthesis of ZnO nanoparticles using *Cymbopogon citratus* aqueous leaf extract: characterization and evaluation of their biological activities

Ahmed S. Abdelbaky[1*], Abir M. H. A. Mohamed[2], Marwa Sharaky[3], Nira A. Mohamed[1] and Yasser M. Diab[1]

Abstract

Background The green synthesis of metal and metal oxide nanoparticles (NPs), notably from plants, has attracted increasing attention in recent years. Although the increased popularity use of *Cymbopogon citratus* as a therapeutic substance, to date, there has not been any research on the chemistry of *C. citratus* aqueous leaf extract (ALE) or synthesis of ZnO NPs utilizing an extract from it. The ecologically safe ALE of *C. citratus* was employed in this study as a bio-reducing and capping agent to synthesize ZnO NPs.

Results The novelty of the current study is the investigation of the antioxidant, anti-inflammatory, anti-microbial, and cytotoxic potencies of biosynthesized ZnO NPs utilizing *C. citratus* ALE. Zinc acetate dihydrate was used as the precursor and the leaf extract serves as the reducing agent. ZnO NPs from ALE of *C. citratus* were characterized by the spherical in form by using high-resolution transmission electron microscopy (HR-TEM) and the Scherrer formula was used to calculate the size of the crystalline structure. The presence of numerous functional groups in both the ALE and the NPs is confirmed by FTIR analysis. The highest absorption peak is observed at 370 nm. The stability and particle size of the biosynthesized ZnO NPs are demonstrated by dynamic light scattering (DLS) analysis. The biosynthesized ZnO NPs exhibited excellent antioxidant activity with an IC_{50} value of 45.67 ± 0.1 µg/mL and exerted interesting anti-inflammatory activity (98.1% ± 0.04) when compared to the standard indomethacin (92.1% ± 0.07) at 1 mg/mL. They also showed anti-microbial activity for both bacterial and fungal which growth rates for both significantly decreased with the increase in ZnO NPs concentration compared to the control. The anticancer activity of biosynthesized ZnO NPs and *C. citratus* ALE was in vitro tested against seven human cancer cell lines (HCCL) (i.e. H1299, MDA-MB-468, HNO97, HEK, HCT116, HuH7, and HEPG2) compared to normal cells (HSF) using the sulforhodamine-B (SRB) assay. More interestingly, the biosynthesized ZnO NPs displayed remarkable selective cytotoxicity against all tested cancer cell lines without any effect on normal cells. In contrast, the cancer cell lines were not affected by the ALE of *C. citratus* at any concentrations tested.

Conclusions All the findings confirm that the ZnO NPs biosynthesized in the current work are promising candidates for a variety of biological activities, and as a result, they can be helpful to the medical sector, environmental and agricultural applications.

Keywords ZnO NPs, Green synthesis, Antioxidant, Antimicrobial, Anti-inflammatory, Cytotoxicity

*Correspondence:
Ahmed S. Abdelbaky
asm03@fayoum.edu.eg
Full list of author information is available at the end of the article

Graphical Abstract

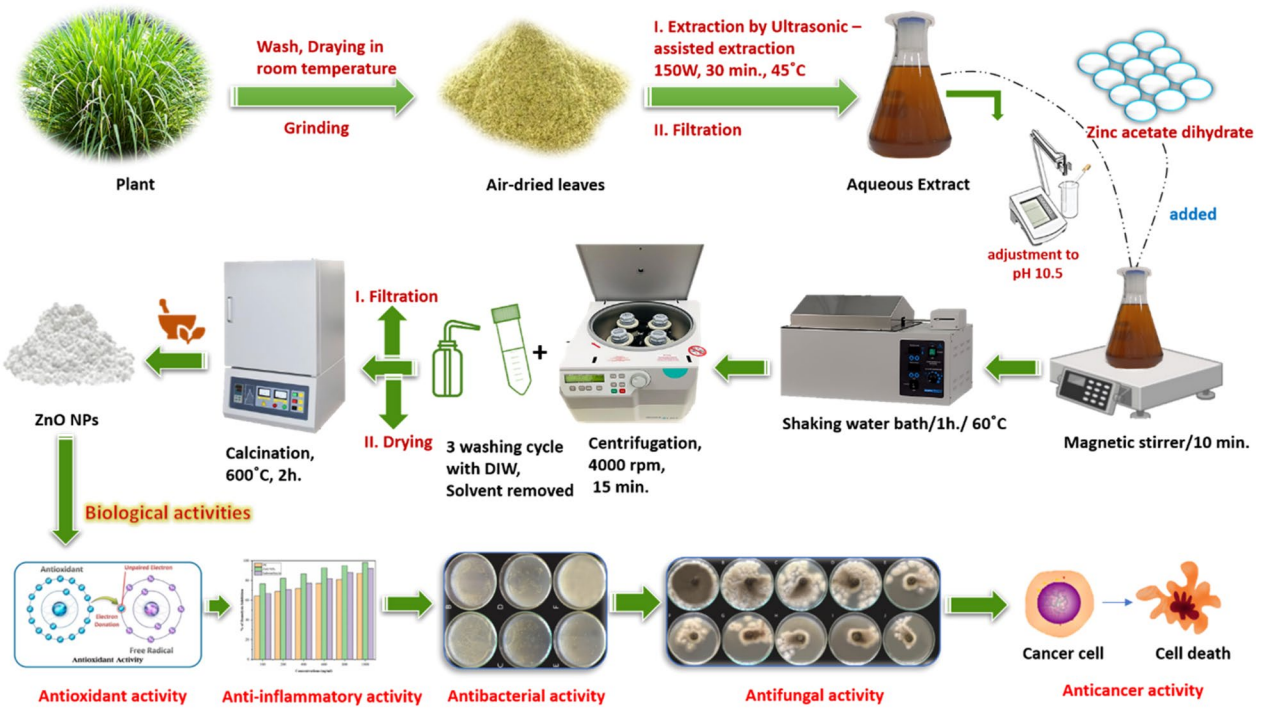

Background

Nowadays, one of the most interesting fields of research in the twenty-first century is nanotechnology (NT) which has caused a paradigm change in the life sciences on a worldwide scale because it created new possibilities for the enhancement of products used in the food industry, cosmetics, healthcare, medicine (diagnosis and treatment for various diseases) [1–3] and NT are currently employed as food sensors to assess the safety and quality of food [4]. Nanoparticles (NPs) are the building blocks responsible for nanotechnology's applicative properties. NPs are very important because they have superior physico-chemical and biological characteristics compared to the bulk material. These NPs materials have a larger surface-to-volume ratio due to their small size (1–100 nm) [5–8], which results in increased surface reactivity [9]. This special characteristic allowed them can be used in a variety of applications from material science to biotechnology [10, 11]. In order to produce these NPs, there are three techniques including physical, chemical and biological approaches [12, 13].

Yet, researchers much choose the biological method because there are many drawbacks of physical and chemical methods such as using a lot of energy, producing hazardous chemicals, expensive, long-term processing and the reactant chemicals used are toxic to the environment, the life of flora and the living system [12, 14]. Additionally, biological methods are preferred over physical and chemical approaches because of their eco-friendliness, ease prepared, non-toxic, economic and produces large quantities with clearly specified sizes and morphologies [15, 16]. Due to these limitations, the majority of the pertinent research has focused on eco-friendly and quick synthesis techniques for the production of NPs.

In response to these challenges, here we utilized plant-derived extracts (green synthesis) instead of synthetic chemical agents as a developing trend possessing the many features mentioned above to biosynthesize metal oxide (MO) NPs for various purposes and overcoming the limitations of physico-chemical methods of NPs synthesis [17–21].

Plants have a diversity of bioactive substances including phenols, flavonoids (Flv.), terpenoids, alkaloids, proteins,

carbohydrates, vitamins and enzymes that can take the role of chemical reagents in the reduction of metal ion into lower valence state [22–24]. The main factors affecting the end-use of NPs in the industry are the kind and nature of the metal utilized for NPs biosynthesis. Several metal and MO NPs of zinc, copper, iron, gold, silver and cerium and many others have recently attracted attention due to their distinctive physical, chemical, and biological characteristics [25–27].

Among these MO NPs, zinc oxide (Zn–O) NPs are widely preferred because of their nontoxicity (generally recognized as safe (GRAS)) and the ability to be used as sunscreen and in cosmetic products due to their high UV-adsorption capacity [28–30]. Additionally, owing to the unique characteristics of ZnO NPs including broad bandgap, high electron mobility and great visible transparency, ZnO NPs are regarded as excellent semiconductors. Furthermore, in the industry of textile, ZnO NPs are added to final fabrics to improve their resistance to UV radiation, antibacterial, and deodorant properties [31]. Also, ZnO NPs can be utilized to remove contaminants from the environment by photodegradation (especially wastewater treatment). As a part of the applications, ZnO NPs can also use for solar cells, electronics, antifungal, pharmaceutical and clinical purposes for treating infectious illnesses in both humans and animals [32–34]. ZnO NPs have recently been validated for use as dietary supplement additives to enhance immunological function, increase antioxidant activity, improve egg quality, and increase layer chicken production [35].

Cymbopogon citratus, also known as lemongrass, belonging to the genus *Cymbopogon*, is commonly grown in tropical countries. One of the primary sources of essential oils for use in medicinal purposes is this species. Lemongrass has a long history of use in several biological activities including the treatment of gastrointestinal disorders [36], oxidative stress, particularly lipid peroxidation [37], antifungal [38], insecticidal [39], cytotoxic activities [40], antioxidant [41], anxiolytic, hypotensive, antidepressant due to a pleasant aroma present in this plant after an infusion [42], antispasmodic, analgesic, antiemetic, antitussive, antirheumatic, and antiseptic [36, 43]. Additionally, other investigations described the traditional uses of lemongrass (*Cymbopogon citratus*) in different countries, including Brazil, Cuba, Egypt, Indonesia, Malaysia, Thailand and the USA where the tea made from its leaves is used as an antispasmodic, diuretic, antipyretic, sedative, hypotensive for catarrh and rheumatism, renal antispasmodic, healing wounds and bone fractures [44].

The phytochemical analyses of *C. citratus* revealed that its leaves are a rich source of several secondary metabolites like polyphenols, tannins, alkaloids, steroids, glycosides, saponins, oils, proteins, fats and carbohydrates [43, 45], which can help the biosynthesis and formation of NPs by acting as reducing, capping or stabilizing agents.

So far, there are no scientific studies on the characterization and biological activities of ZnO NPs synthesized by *C. citratus* ALE. The objective of the present study was to successfully investigate the in vitro antioxidant, antibacterial, antifungal, anti-inflammatory and cytotoxic activities of ZnO NPs prepared by using *C. citratus* ALE along with providing a new, easy and eco-friendly green route for the biosynthesis of ZnO NPs using *C. citratus* ALE assisted with ultrasonic extraction as a reducing agent and an effective stabilizer, instead of harmful, reducing and expensive stabilizing chemicals like surfactants and polymers. The identification and quantification of phenolic compounds including flavonoids in *C. citratus* ALE were also studied using HPLC.

Materials and methods

Plant collection

Cymbopogon citratus fresh leaves were collected in the month January 2021 from the Abu-Junshu botanical garden, Abshway, Fayoum, Egypt. The leaves were air-dried and subsequently ground to powder by a laboratory blender (Bosch, 1600w, USA) and maintained until needed in a sealed container at ambient air temperature (28 ± 2 ℃) and away from light.

Chemicals and reagents

All chemicals and reagents in the current study acquired were analytical grades, and in particular, zinc acetate dihydrate (Advent, Navi Mumbai, India), 1,1 diphenyl-2-picrylhydrazyl (DPPH, > 99%) and L-ascorbic acid (Sigma-Aldrich, St. Louis, MO, USA), Luria broth (LB), potato dextrose agar (PDA) and amoxicillin (HiMedia, Mumbai, India), methanol (Merck, USA) were used without additional purification. Deionized water (dH_2O) was used during the biosynthesis process.

Preparation of *C. citratus* ALE

A 50 g of dried powdered leaves of *C. citratus* was added to 500 mL (1:10 ratio, w/v) of deionized water (DIW) (Milli Q, Millipore, Molsheim, France) in an Erlenmeyer flask. The flask containing the respective dried leaves was placed in an ultrasonic probe homogenizer (Benchmark, 150 W, USA) at 45 ℃ for 30 min. The solid residues from the extract were removed by centrifugation (Hermle Z 366 K, Wehingen, Germany) at 4000 rpm for 15 min until a clear filtrate was obtained and the filtrate was used for ZnO NPs synthesis.

HPLC analysis

An Agilent 1260 series was used for the HPLC analysis. Eclipse C18 column (4.6 mm × 250 mm i.d., 5 µm) was employed for the separation. Water (A) and 0.05% trifluoroacetic acid (TFA) in acetonitrile (B) were the components of the mobile phase, which had a flow rate of 0.9 mL/min. The following time intervals for the mobile phase were set in a linear gradient: 0 min (82%, A); 0–5 min (80%, A); 5–8 min (60%, A); 8–12 min (60%, A); 12–15 min (82%, A); 15–16 min. (82%, A) and 16–20 min. (82%, A). At 280 nm, the multi-wavelength detector (MWD) was observed. For each of the samples, 5 µl of injection volume was used. The temperature in the column was set constant at 40 ℃.

Biosynthesis of ZnO nanoparticles (ZnO-NPs)

Twenty millilitres of collected *C. citratus* filtrate was added dropwise to 50 mL of 0.1 M zinc acetate di-hydrate (Mw = 219.49 g/mol) under vigorous stirring at 60 ℃ for 1 h. The pH was adjusted to 10.5 by using NaOH (2 ml, 0.5 M) as the starting material. After that, was monitored the resultant solution using UV-double beam spectroscopy (Hitachi, Tokyo, Japan) until the appearance of a light-brown precipitate. The resultant obtained (precipitate) was centrifuged (Hermle Labortechnik Gmbh Z 366 K, Wehingen, Germany) for 15 min at 4000 rpm and the precipitate was washed three times with DIW. The supernatant was discarded after centrifugation, and the precipitates were collected, dried and calcined for two hours at 600 ℃ in a muffle furnace to produce the desired product in the form of a white powder.

Characterization of ZnO-NPs

Ultraviolet–visible (UV–Vis) analysis

The UV–Vis absorbance of ZnO NPs was tested to determine the bandgap energy and demonstrate that the NPs were successfully synthesized. Briefly, 0.01 g of ZnO NPs was dispersed in double-distilled water (DDW) by Sonicator (Branson, Milford, USA), then 2 mL in a quartz cuvette was taken and analysed using UV–Vis Hitachi spectrophotometer U-2900 over the wavelength scan of 200–700 nm.

Zeta potential analysis

The zeta potential (ZP) values were determined by Zetasizer (Malvern ZS, UK) to investigate the stability of biosynthesized nanoparticles.

Fourier transform infrared (FTIR) analysis

The functional groups involved in the biosynthesis of ZnO NPs with a spectrum range of 4000–400 cm^{-1} were identified using FTIR analysis (Brüker, Berlin, Germany).

X-ray diffraction (XRD) analysis

XRD analysis (Brüker D8 DISCOVER, Germany) was used to determine the crystallinity and purity of the obtained ZnO-NPs.

Energy dispersive X-ray analysis (EDX)

The elemental structures of the biosynthesized ZnO-NPs were measured by the energy-dispersive spectroscope (EDX, Brüker, Germany) to detect the elemental compositions of different NPs.

High-resolution transmission electron microscopy (HR-TEM)

The morphology of the biosynthesized ZnO-NPs including the shape and size were examined by HR-TEM (JEÖL, JEM-2100, Japan) at a 200 kV accelerated voltage.

Biological activities of C. citratus-mediated biosynthesis of ZnO-NPs

Antioxidant activity

The DPPH test, previously reported by Brand-Williams et al. [46], was utilized to assess the free radical scavenging activity (FRSA) of biosynthesized ZnO NPs and the ALE of *C. citratus*. Briefly, 2 mL of DPPH (Sigma-Aldrich, Louis, USA) solution was added to 50 µl of ZnO NPs and the ALE of *C. citratus* separately at concentrations of 1000, 500, 250, 100, 50, 25 and 12.5 µg/mL. The reaction mixture was thoroughly stirred before being let to stand for 30 minutes in the dark at room temperature (35 ± 2 ℃) to protect the mixture from light radiation. The decrease of the DPPH radical was assessed by measuring the absorbance at 517 nm after 30 min. To calibrate the resulting activity, L-ascorbic acid was employed as a reference material. The following equation was used to determine the FRSA, which is expressed as a percent inhibition of the DPPH radical:

% Inhibition (% FRSA) = $[(A_{DPPH} - A_{sample}) / A_{DPPH}] \times 100$, where A is the absorbance. The relationship between sample curve and the corresponding FRSA concentrations was used to calculate the IC_{50} values.

Antimicrobial activity

Microbial strains and culture conditions In this study, three pathogenic microorganisms were chosen, including two foodborne pathogenic bacteria [G(+) *Staphylococcus aureus* ATCC 8095, and G(−) *Pseudomonas aeruginosa* ATCC10662] and one fungal plant pathogen (*Aspergillus niger* AUMC3663). The two bacterial isolates were taken from Agricultural Microbiology Department, Fayoum

University, Egypt, while the fungal strain was obtained from Mycological Centre (AUMC), Assiut University, Egypt. *S. aureus* and *P. aeruginosa* were sub-cultured in Luria–Bertani (LB) broth medium (Hi-Media, Mumbai, India) containing 0.1% tween 80 in a shaking incubator at 37 ℃ for 24 h at 150 rpm whereas *A. niger* was sub-cultured on potato dextrose agar (PDA) plates (Himedia, Marg, Mumbai, India) for 7 days at 30 °C until normal sporulation is achieved.

Antibacterial assay, MIC and MBC determination

The antibacterial activity of ZnO NPs was evaluated against *S. aureus* (ATCC 8095) and *P. aeruginosa* (ATCC10662) strains by total viable count (TBC) method. Four various concentrations (25, 50, 100, and 200 µg/mL) of biosynthesized powder ZnO NPs were resuspended individually in 10 mL LB broth and subjected to an ultrasonic probe homogenizer (Benchmark, 150 W, USA) for 10 min. Following that, each was autoclaved and ready until use. 400 µL of freshly prepared bacterial strain cultures overnight containing (10^7 CFU) was added for each concentration. Untreated bacterial cultures were used as control. Subsequently, they were incubated under shaking at 150 rpm for 24 h. Finally, 10 µL of bacterial cultures were spread on LB plates after proper dilution for the cultures and incubated overnight, then colonies were counted to determine the minimum bactericidal concentration (MBC) which was detected as the least concentration of the biosynthesized ZnO NPs that inhibited bacterial growth on plates. Optical density was measured compared with the control. Thrice the experiment was repeated. The minimum inhibitory concentration (MIC) was determined as the lowest concentration of biosynthesized ZnO NPs that exhibited no visible growth of the bacterial cells which was measured by taking optical density at 600 nm by using UV-spectrophotometer (Hitachi U2900, Tokyo, Japan) after 24 h incubation. Growth inhibition percentage was done by comparing with the control utilizing the given equation:

$$\mathrm{I}\% = \frac{\mu\mathrm{C} - \mu\mathrm{T}}{\mu\mathrm{C}} \times 100,$$

where I% = inhibition percentage of bacterial growth; µC = mean value of $\mathrm{O.D.}_{600}$ in control, µT = mean value of $\mathrm{O.D.}_{600}$ in treatment.

Antifungal activity test

The antifungal activity of biosynthesized ZnO NPs towards *A. niger* at various concentrations (25, 50, 100, 150, 200, 250, 500, 1000 and 2000 µg/mL) was studied to assess the antifungal effect by using the poison food technique approach [47]. Briefly, a PDA medium with the above-mentioned concentrations of biosynthesized ZnO NPs was prepared separately, and homogeneous mycelial discs (4 mm diameter) were collected from the edge of a 7-day-old *A. niger* culture and were placed in the centre of each petri plate and incubated for 5 days at 30 ℃. The percentage of mycelium growth inhibition (MGI) was determined according to the formula:

$$\mathrm{MGI}(\%) = \frac{\text{Mycelial growth}_{(\text{control})} - \text{Mycelial growth}_{(\text{treatment})}}{\text{Mycelial growth}_{(\text{control})}} \times 100.$$

Mycelium growth was assessed by measuring the horizontal and vertical diameters of the colony in each plate according to Soylu et al. [48].

Anti-inflammatory activity

Erythrocyte suspension preparation

Fresh whole blood (3 mL) was obtained from the blood bank, at Fay. Uni. Hospital, and centrifuged at 3000 rpm for 10 min in heparinized tubes. The normal saline volume used to dissolve the red blood pellets (RBP) was equal to the volume of the supernatant. The volume of the dissolved RBP collected was estimated and reconstituted as a 40% (v/v) suspension together with isotonic buffer solution (10 mM sodium phosphate buffer (Na-PB), pH 7.4). The Na-PB contained 1.15 g of Na_2HPO_4, 0.2 g of NaH_2PO_4, and 9 g of NaCl in one litre of DDW. The reconstituted RBCs (resuspended supernatant) were employed as such.

Hypotonicity-induced haemolysis

In this test, the ALE and NPs used were dissolved in DDW (hypotonic solution). In duplicate pairs of centrifuge tubes, the hypotonic solution (5 mL) containing graduated dosages of the aqueous extract and NPs (100, 200, 400, 600, 800, and 1000 µg/mL) was added (per dose). In addition, isotonic solution (5 mL) containing graded dosages of the aqueous extract and NPs (100—1000 µg/mL) was added to duplicate pairs (per dose) of centrifuge tubes. Five millilitres each of DDW and indomethacin 200 µg/mL made up the control tubes. To each of the tubes, 0.1 ml of

erythrocyte suspension was added and mixed gently. The mixtures were kept for 1 h at room temperature (37 ℃) before being centrifuged at 1300 *g* for 3 min. A Spectronic (Hitachi, Tokyo, Japan) spectrophotometer was used to assess the absorbance (O.D.) of the supernatant's haemoglobin content at 540 nm. By assuming that all heamolysis produced in the presence of distilled water (DW) is 100%, the percentage heamolysis was estimated. The percent inhibition of haemolysis by the extract and ZnO NPs was determined using the following formula:

$$\text{Inhibition of haemolysis}(\%) = 1 - \frac{(A_2 - A_1)}{(A_3 - A_1)} \times 100,$$

where A_1 is the absorbance of the test sample (TS) in an isotonic solution (IS); A_2 is the absorbance of TS in a hypotonic solution (HS); and A_3 is the absorbance of the control sample in HS.

In vitro *cytotoxic efficacy of biosynthesized ZnO NPs by C. citratus leaf extract*

Human cancer cell lines

Human lung cancer cell lines (H1299), human breast cancer cell line (MDA-MB-468), human oral squamous cell carcinoma (HNO97), human embryonic kidney (HEK), human colon cancer cell line (HCT116), hepatocarcinoma cell line (HuH7), liver hepatocellular carcinoma cell line (HEPG2) and human splenic fibroblasts (HSF) were acquired from the American Type Culture Collection (ATCC, Minnesota, USA) and were kept at Pharmacology Unit—Cancer Biology Department, National Cancer Institute (NCI), Cairo, Egypt, in Dulbecco's modified Eagle medium (DMEM) containing 10% foetal bovine serum, 0.2% sodium bicarbonate and 1% penicillin–streptomycin. Every cell line was routinely incubated at 37 ℃ with 5% CO_2 in a humidified atmosphere.

Cytotoxicity assay

The cytotoxic effect of the *C. citratus* ALE and ZnO NPs towards all tested cancer cell lines cells were assessed using sulforhodamine-B (SRB) assay [49]. Briefly, on 96-well microtiter plates, cells were seeded at a density of 3×10^3 cells/well. They were left to attach for 24 h prior to being incubated with *C. citratus* ALE and ZnO NPs, respectively; followed by the treatment of the cells with concentrations values of 62.5, 125, 250 and 500 µg/mL for H1299, MDA-MB-468, HNO97, HEK, HCT116, HuH7 and HEPG2, and HSF cells. Each concentration was tested in triplicate, and the incubation period was extended to 48 h. Using DMSO as a control vehicle (1% v/v). After 48 h, cells were treated with 20% trichloroacetic acid (TCA) to be fixed, and stained with 0.4% SRB dye. Using an ELISA microplate reader (TECAN sun-rise™, Germany), optical density (O.D.) of each well was measured at 570 nm. According to the following formula: the O.D. of the treated cells divided by the control cell's O.D., the mean survival fraction was calculated for each extract concentration.

Statistical analysis

All trials (antioxidant, antimicrobial, anti-inflammatory and anticancer activities) were carried out with 3 replications of each concentration. The obtained data were analysed using the two-way ANOVA method to find significant differences in antioxidant activity, different bacterial and fungal strains, anti-inflammatory and cytotoxic effects, which was then followed by Duncan's multiple-range tests. All findings were examined using the SPSS® IPM® statistical software (version 23, New York, USA).

Results and discussion

Effect of plant extract (PE) concentration on biosynthesis of ZnO NPs

The concentration of PE plays an important role in the biosynthesis of ZnO NPs. It has been found that the ideal ratio of PE to zinc acetate dihydrate (ZAD) for the biosynthesis of ZnO NPs was 20 mL/g (i.e. 1 g of ZAD in 20 mL of PE). The yield of ZnO NPs was lower when using 5, 10 and15 mL (PE)/g (ZAD) due to an insufficient amount of bioactive components present in these volumes, whereas 20 and 25 mL/g yielded approximately the same higher amounts of ZnO NPs. That means the concentration of the bioactive components found in the case of 20 mL/g was adequate to reduce every Zn^{2+} ion found in the reaction mixture.

Characterization of ZnO NPs

Visual observation

The visual examination confirmed the preliminary formation of ZnO NPs. When *C. citratus* ALE was added to the ZAD, the colour of the ALE was changed from pale red to light brownish precipitate (ppt.) (Fig. 1) during the reaction, demonstrating the biosynthesis of ZnO nanoparticles. There are three main stages in the mechanism of synthesis: (1) the activation stage during which the zinc ions in respective salt solutions (ZAD) are bound to the reducing metabolites and stabilizing agents present in the ALE of *C. citratus* and are reduced to zinc atoms and nucleation of the reduced zinc atoms; (2) the growth stage known as Ostwald ripening, during which nearby small NPs spontaneously coalesce into larger particles; this process involves heterogeneous nucleation, growth, and additional Zn ion reduction; it also results in an

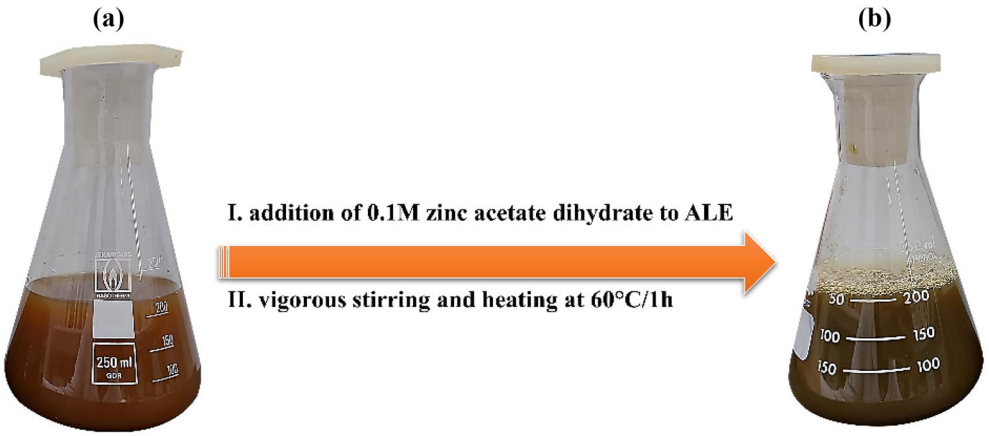

Fig. 1 The visual colour changes that occur visually at zero-time (**a**) ALE of *C. citratus* and after 1 h (**b**) ALE of *C. citratus* and ZAD

increase in the thermodynamic stability of the NPs; and (3) the termination stage determines the final shape of the NPs and then after oxidizing, well-dispersed and stable ZnO NPs can be formed [50–55]. Figure 2 depicts a schematic representation of the formation of NPs.

UV–visible spectroscopy

In order to investigate the optical absorption property of the biosynthesized ZnO NPs, the UV–visible absorbance spectra were monitored at room temperature in the wavelengths of 200 to 700 nm and are illustrated in Fig. 3. From the observed results in Fig. 3, the highest absorption peak at 370 nm confirmed the synthesis of ZnO NPs via the green route which is matched to the characteristic band of ZnO NPs [56, 57]. Furthermore, the observed absorption spectra of biosynthesized ZnO NPs exhibited a sharp and intense peak in the UV region at 370 nm, which corresponds to the absorption spectrum of earlier described ZnO NPs, as mentioned in Kayani et al. [58]. This is the characteristic absorption peak of ZnO.

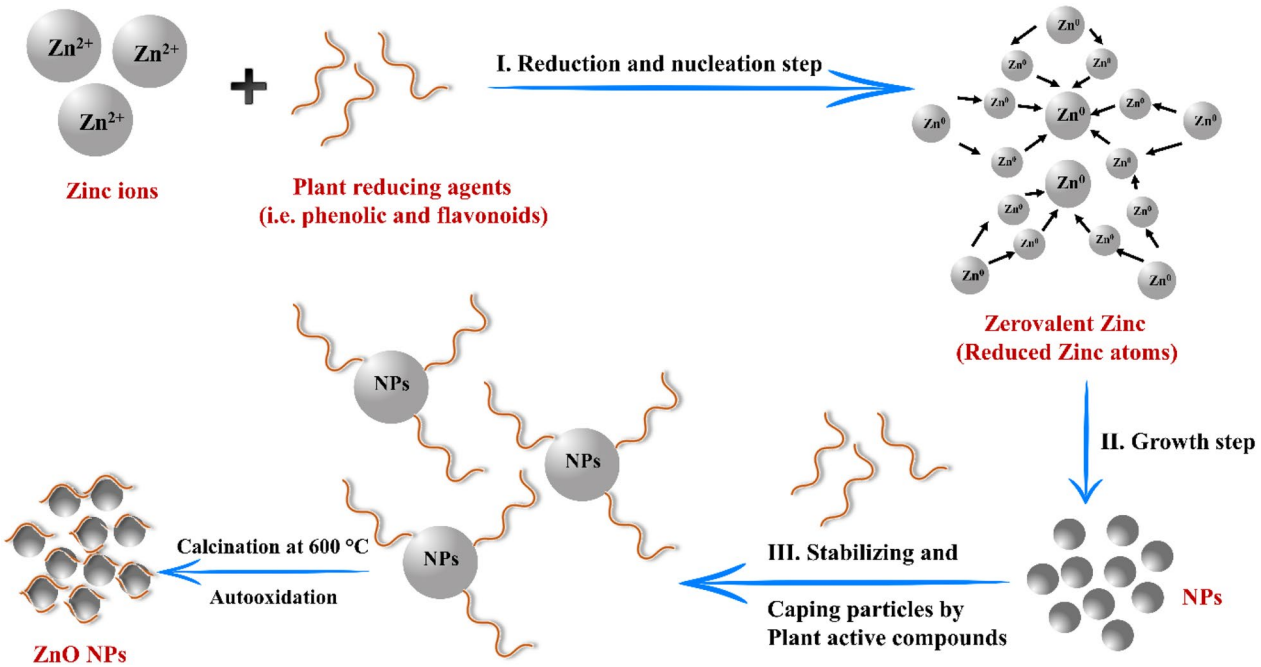

Fig. 2 Formation mechanism of ZnO NPs utilizing plant extract

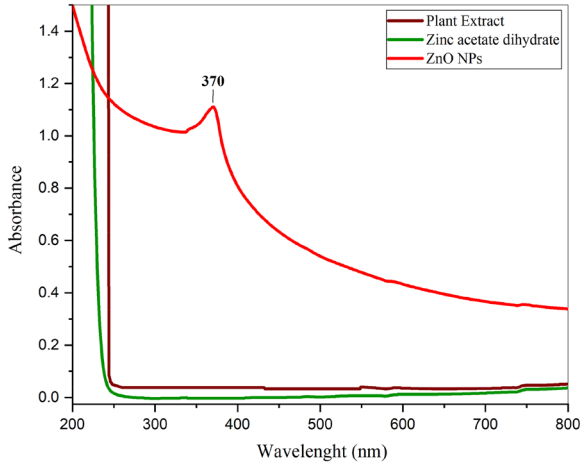

Fig. 3 UV–Vis spectrum of biosynthesized ZnO NPs

Dynamic light scattering (DLS) analysis

Particle size (PS) was measured by the DLS method (a common approach for determining the size of particles in colloidal solutions) using Zetasizer (Malvern, UK). The instrument has a sensitivity for molecular weight (MW) below to 250 Da and can measure PSs of samples suspended in liquids with concentrations ranging from 0.00001% to 40%. Using this technique, the polydispersity index (PDI), size distribution (SD), and average particle size (APS) of the biosynthesized ZnO NPs were assessed and the findings are displayed in Fig. 4. As depicted in Fig. 4, the resulting PS of ZnO NPs exhibits an average size (nm) of about 28 nm. The polydispersity index (PDI) of the ZnO NPs is 0.198. This result is entirely consistent with the findings of Badran, and Dina et al. [59, 60], who stated that polydispersity index values of 0.3 and less are regarded as monodisperse.

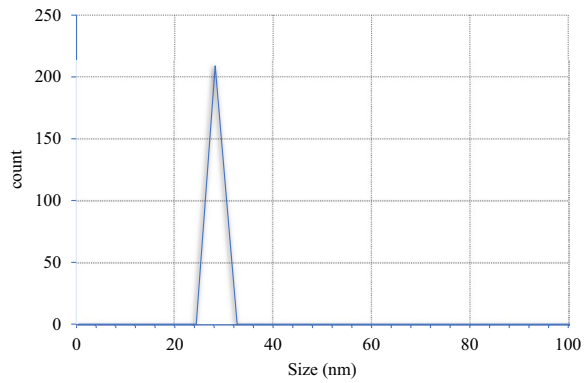

Fig. 4 Particle size distribution (PSD) of biosynthesized ZnO NPs

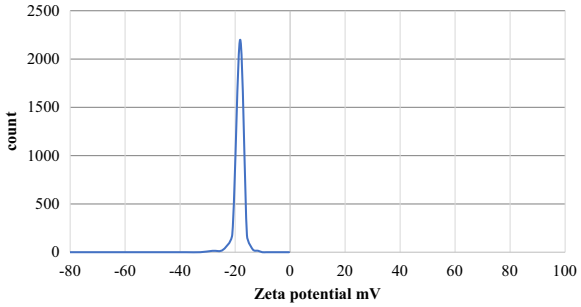

Fig. 5 Zeta potential (ZP) analysis of biosynthesized ZnO NPs

Zeta potential analysis

In order to determine the surface charges that ZnO NPs acquired, a zeta potential (ZP) analysis was conducted. This analysis can be utilized to learn more about the stability of the colloidal ZnO NPs that were obtained. The stability of the nanoparticles in the solution is correlated with their ZP. If the particles in a suspension have strong (−) or (+) ZP values there will not be any aggregation of nanoparticles since they will repel one another. In contrast, if particles have small ZP there is no force to stop particles from aggregating and joining together. ZP values larger than (+30 mV) or lower than (− 30 mV) are typically considered to produce stable suspensions [61]. Water was used as a dispersant to measure the ZP of the biosynthesized ZnO NPs. In our study, as illustrated in Fig. 5, the ZP was observed to be − 20 mV. The highly negative ZP value confirms the repulsion between the particles and thus enhances the stability of the formulation [62].

Energy dispersive X-ray diffractive (EDX) analysis

To know the elemental composition of the biosynthesized ZnO NPs, the EDX analysis was employed. The zinc and oxygen signals of ZnO NPs are confirmed by the EDX elemental mapping and the distribution of zinc is homogeneous as displayed in Fig. 6. The elemental analysis of the nanoparticle revealed 83.60% zinc and 16.40% oxygen, demonstrating the maximum level of purification for the produced nanoparticle.

FTIR analysis

The functional groups (FGs) present in *C. citratus*-mediated ZnO NPs synthesis were identified using FTIR spectroscopy. The resulting spectra of biosynthesized ZnO nanoparticles and *C. citratus* ALE are shown in Fig. 7 and Table 1 displays the absorption spectra with probable assignments. From Fig. 7, different intense bands were exhibited at 3409.55, 2923.57, 2356.60, 1616.06, 1400.07,

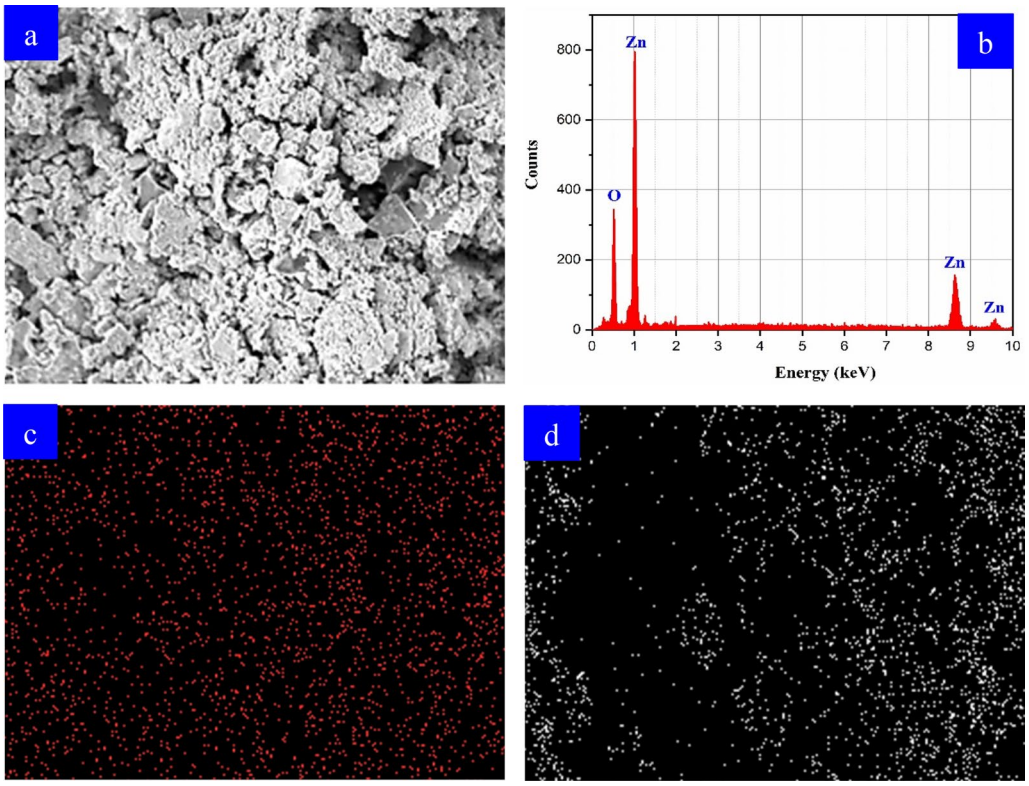

Fig. 6 EDX pattern (**a** and **b)** and elemental mapping of ZnO NPs: **c** Zn, **d** O

1076.09, and 620.97 cm^{-1} and 3424.97, 2923.57, 2356.60, 1619.92, 1403.93, 1091.51, 617.11, and 435.83 cm^{-1} for *C. citratus* ALE and ZnO NPs, respectively. The FTIR spectra showed a broad absorption band in a higher energy region at 3409.55 and 3424.97 cm^{-1} due to the -OH stretching frequency of phenolic and flavonoid components [63–65]. The absorption bands at 2923.57 and 2356.60 cm^{-1} which is characteristic of the –C–H (hydroxyl compound), N–H or the C=O stretching vibrations, respectively [65, 66]. It is possible to attribute the following peaks (1616.06 cm^{-1} and 1619.92 cm^{-1}) to the C=O stretching vibration in the carboxyl group or bending C=N vibration in the amide group [67, 68]. The aromatic –CH stretching vibrations correspond to the observed bands (1400.07 cm^{-1} and 1403.93 cm^{-1}) [65]. The C–O bond stretching of the aromatic rings was revealed by the sharp intensity bands at 1076.09 cm^{-1} and 1091.51 cm^{-1} [69], which may also be correlated to the phenolic and flavonoids [70–72] present in the *C. citratus* extract. The bands at 620.97 cm^{-1} and 617.11 cm^{-1} are corresponding to the C–H out-of-plane bending. Furthermore, the FTIR spectrum revealed a distinct and

Table 1 FTIR spectra with potential assignments for both *C. citratus* ALE and ZnO NPs

Possible assignment	Absorption peaks in *C. citratus* ALE (cm^{-1})	Absorption peaks in ZnO NPs (cm^{-1})
-OH stretching vibrations	3409.55	3424.97
-C-H stretch in alkanes	2923.57	2923.57
N-H or C = O stretching vibrations	2356.60	2356.60
C = O carboxylic group	1616.06	1619.92
–CH aromatic ring	1400.07	1403.93
C-N stretching in amino acids	1076.09	1091.51
-C-H stretch (aromatics)	620.97	617.11
Zn–O	–	435.83

intense band at 435.83 cm^{-1} attributed to Zn–O stretching vibration [63, 73, 74], confirming *C. citratus* ALE is used as a reducing and capping agent in the biosynthesis of ZnO NPs. Consistent with our findings, the FTIR examination of biosynthesized ZnO NPs revealed the absorption band of ZnO has been identified at wavelength 442 cm^{-1} [69], 400 to 500 cm^{-1} [75], 450 cm^{-1} and 600 cm^{-1} [76], 485 cm^{-1} [77]. Furthermore, these findings are compatible with our previous study of green ZnO NPs utilizing *Pelargonium odoratissimum*, which exhibits absorption bands at 430 nm [63].

The FTIR data revealed that phenolic and flavonoid components were the significant compounds in the ALE and ZnO NPs. Hence, FTIR evaluated for ZnO NPs biosynthesized by *C. citratus* ALE (Fig. 7) confirm with the findings of FTIR spectrum of ALE, which demonstrated that the organic substances (i.e. phenols and flavonoid) of *C. citratus* ALE which were calcined during the manufacture of ZnO, still kept their natural characteristics and thereby reduced the ZnO NPs. Additionally, the HPLC technique of the ALE identified 16 phenolic compounds in the proper concentrations depicted in Table 2 and Fig. 8, which could be responsible for the reduction of the metallic ions in salt precursors (zinc acetate dihydrate) into ZnO-nanosize particles, capping, and stabilizations of biosynthesized ZnO NPs. Furthermore, among the numerous important phenolic compounds identified, caffeic acid, methyl gallate, chlorogenic acid, catechin, gallic acid, rutin, coumaric acid and vanillin were shown to be highly abundant. Since their functional (-COOH and -OH) groups are readily ionized, polyphenols [i.e. phenolic acids (PAs) and flavonoids (Flv.)] are both known to be strong hydrogen donors [78, 79], that are involved in a wide range of biological processes [80]. It is probable that the phenolic/flavonoid molecules reacting with Zn^{2+} ions via a donor–acceptor mechanism are the possible mechanism by which ZnO NPs are formed utilizing plant extract. As a result of oxygen or hydroxyl compounds found in the PE tending to contribute an electron to electrophile Zn complexes, OH groups are oxidized and electron-deficient zinc ions are reduced to zinc atoms (Fig. 2) [81].

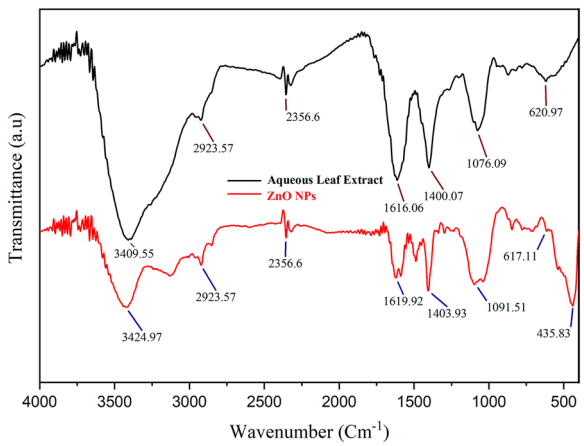

Fig. 7 FTIR spectra of ALE of *C. citratus* and ZnO NPs

X-ray diffraction analysis (XRD)

The XRD pattern of ZnO NPs synthesized by *C. citratus* ALE calcined at 600 °C is illustrated in Fig. 9. The XRD pattern shows 2θ values at 31.85°, 34.55°, 36.35°, 47.69°, 56.75°, 63.09°, 66.56°, 68.17°, 69.29°, 72.87° and 77.21°. Every detected peak observed could be indexed as the ZnO wurtzite structure, which agrees with the JCPDS Data Card No. 36–1451 [82], nanomaterials. Additionally, the absence of any distinctive XRD peaks other than zinc oxide peaks indicates that the produced nanopowder was highly pure and free of impurities [83, 84]. The Debye–Scherrer equation [85] was used to calculate the average crystallite size (D) of the biosynthesized ZnO NPs:

$$D = \frac{0.94\lambda}{\beta \cos\theta},$$

where 0.94 is Scherrer's constant, λ is the X-ray wavelength = 1.5406, θ is the Bragg diffraction angle, and β is the peak full width (FW) of the diffraction line at half-maximum (HM) intensity (FWHM). The APS of the biosynthesized ZnO NPs was found to be 19.01 nm which was determined from the most intense peaks using Debye–Scherrer's formula, and the result is depicted in Table 3.

Table 2 Polyphenolic content (µg/g) of *C. citratus* ALE

No.	Retention time (min)	Compounds	Concentration (µg/g)
1	3.33	Gallic acid	698.37
2	4.18	Chlorogenic acid	1301.30
3	4.60	Catechin	1121.70
4	5.44	Methyl gallate	3616.75
5	5.91	Caffeic acid	3953.37
6	6.57	Syringic acid	45.35
7	7.65	Rutin	856.47
8	8.63	Ellagic acid	104.38
9	9.05	Coumaric acid	632.05
10	9.75	Vanillin	529.71
11	10.21	Ferulic acid	215.83
12	10.43	Naringenin	98.96
13	12.58	Quercetin	119.62
14	14.15	Cinnamic acid	91.17
15	14.88	Kaempferol	155.08
16	15.46	Hesperetin	76.61

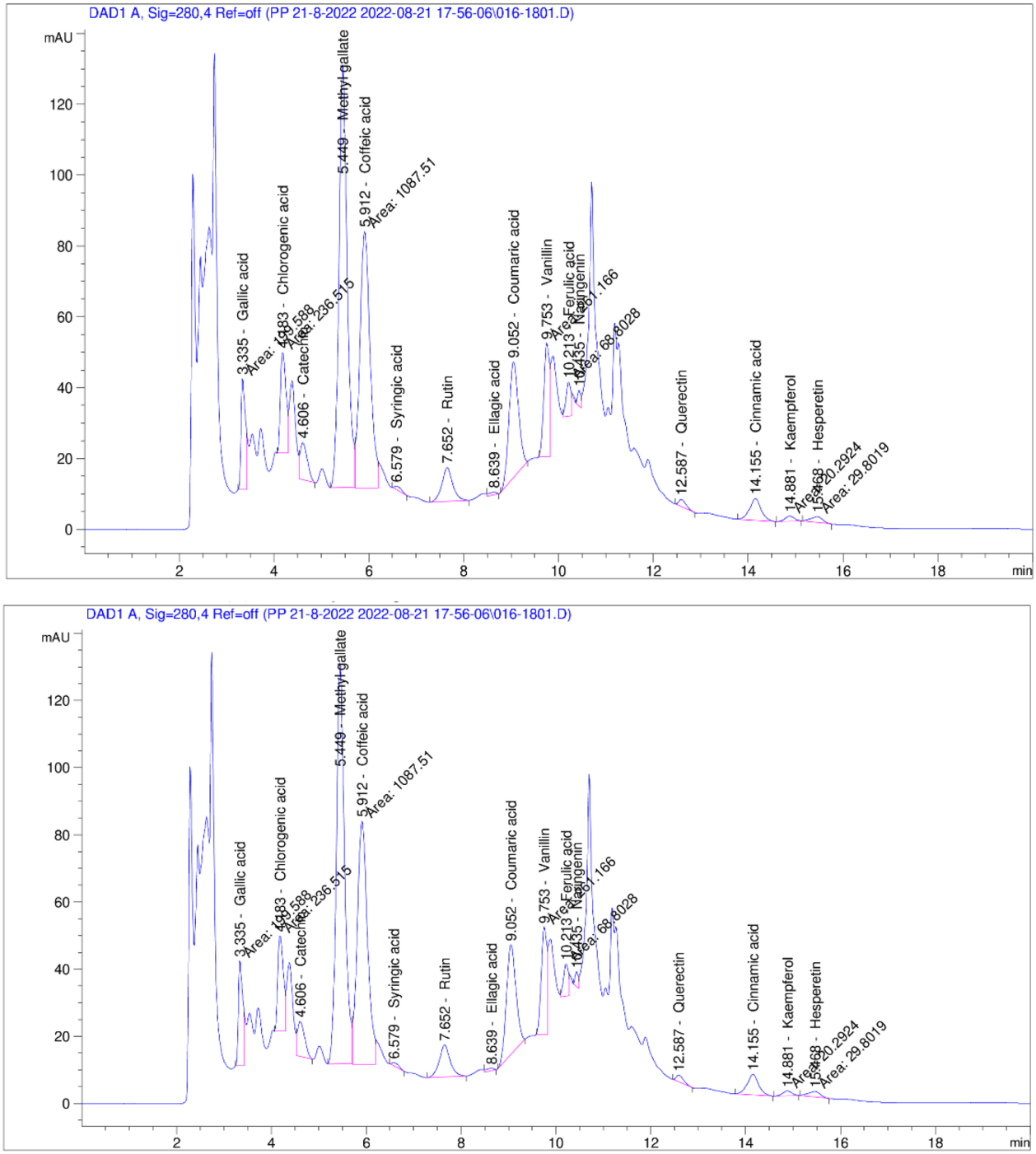

Fig. 8 HPLC chromatogram of **a** standard phenolic and flavonoid compounds and **b** *C. citratus* ALE

High-resolution transmission electron microscopy (HR-TEM)

To confirm the formation of green synthesized ZnO NPs, an HR-TEM examination was carried out. Figure 10A-D and F displays the size, size distribution, as well as shape of ZnO NPs mediated *C. citratus* without any aggregation. The HR-TEM micrographs display the biosynthesized ZnO NPs were spherical in form and had an average mean size of 21 nm (Fig. 10F). Moreover, the selected area electron diffraction (SAED) pattern (Fig. 10F) demonstrated a sequence of rings with bright spots, indicating that ZnO NPs synthesized via *C.*

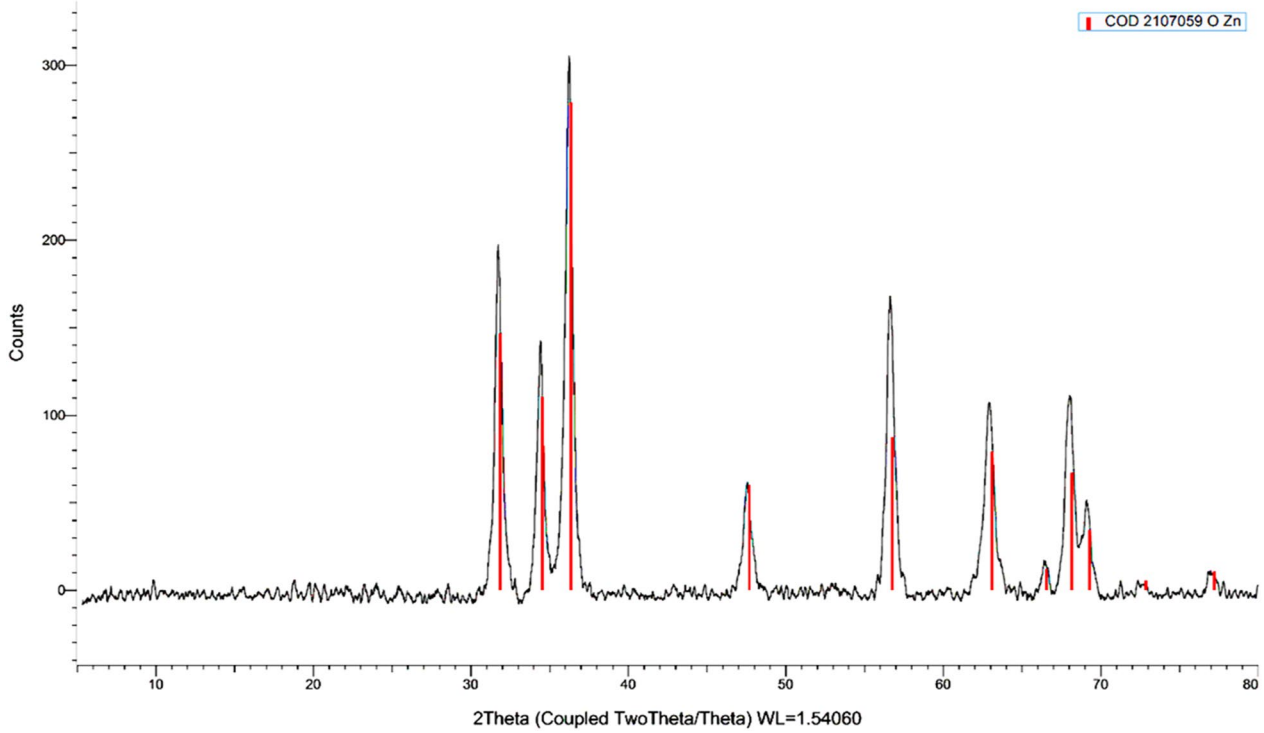

Fig. 9 XRD pattern of ZnO NPs synthesized via *C. citratus* ALE

citratus ALE are crystalline in nature. The particle size acquired by the HR-TEM study closely matches the (D) of ZnO identified through XRD analysis.

Bioactivities of biosynthesized ZnO NPs

Antioxidant activity

Antioxidants protect cells from reactive oxygen species (ROS) harmful effects. Due to their ability to prevent disease and improve health, natural antioxidants have recently become very popular [86]. It is generally known that due to the complexity of phytochemicals, there are various ways to assess the antioxidant capabilities of PEs [87]. DPPH is considered a rapid and easy technique for determining the FRSA of biosynthesized ZnO NPs. The reduction by ZnO NPs results in a colour change from purple to yellow, which is further supported by a decrease in absorbance at 517 nm [88]. The antioxidant activity of biosynthesized ZnO NPs and *C. citratus* ALE was increased with a concentration increase from 12.5 µg/mL to 1000 µg/mL (Fig. 11). The highest antioxidant activity at 50 µg/mL noted for the L-ascorbic acid (60%), followed by ZnO NPs (54%) relative to the ALE of *C. citratus* (18%). This antioxidant value of the ZnO NPs biosynthesized by ALE of *C. citratus* was shown to be better than the values mentioned by Rajakumar et al. [89] for leaf extract of *Andrographis paniculata* (62% at 500 µg/mL), and by Nagajyothi et al. [88] for root extract of *Polygala tenuifolia* (45.47% at 1000 µg/mL). As shown in Fig. 11, the greatest antioxidant activity was obtained in the L-ascorbic acid with the lowest IC_{50} of 30.14 ± 0.04 µg/mL, followed by the ZnO NPs, with 45.67 ± 0.1 µg/mL and ALE of *C. citratus* with 200 ± 0.1 µg/mL. Moreover, this IC_{50} value of biosynthesized ZnO NPs was discovered to be a stronger antioxidant than the ZnO NPs biosynthesized by tuber extract of *Coccinia abyssinica* [90], whose IC_{50} value was 127.74 µg/mL. Additionally, our biosynthesis of ZnO NPs displayed superior antioxidant properties when tested using the DPPH assay compared to its ALE of *C. citratus*. The antioxidant properties of ZnO NPs may be due to the transfer of electron density from the oxygen to the odd electron on the nitrogen atom in DPPH. This feature dependent on the configuration structure of oxygen atom, and it determines the thermal stability of NPs by its accessible free energy (FE) of the oxides [91]. In summary, our results support the findings of Khan et al. [92], who stated that the green synthesized ZnO NPs exhibited strong antioxidant activity as a result of their charge density and surface capping materials.

Antibacterial activity

Antibacterial effects of biosynthesized ZnO NPs, *C. citratus* ALE, and amoxicillin as a positive control against G(+) *S. aureus* (ATCC 8095) and G(−) *P. aeruginosa* (ATCC10662) bacteria were investigated by using total

Table 3 FWHM values and crystallite average sizes calculated using Scherrer's equation of ZnO NPs synthesized via *C. citratus* ALE

h	*k*	*l*	2*θ* (degree)	*d*-spacing (d_{hkl})	FWHM (degree)
1	0	0	31.850	2.80740	0.3403
0	0	2	34.552	2.59380	0.3542
1	0	1	36.358	2.46900	0.3771
1	0	2	47.699	1.90510	0.4212
1	1	0	56.752	1.62080	0.4064
1	0	3	63.094	1.47230	0.3169
2	0	0	66.565	1.40370	0.3488
1	1	2	68.170	1.37450	0.3623
2	0	1	69.290	1.35500	0.4782
0	0	4	72.876	1.29690	0.4482
2	0	2	77.214	1.23450	0.4021
Crystallite average size					19.01 nm

viable count technique, which is illustrated in Fig. 12. Figure 13 summarizes the number of both *S. aureus* and *P. aeruginosa* colonies expressed as the logarithm (log) of the CFU in the presence of ZnO NPs with various concentrations.

It was observed from Figs. 12 and 13 that the log of CFU of *S. aureus* growth grown in the presence of green ZnO NPs has decreased at all concentrations in comparison to the control sample of bacteria while *C. citratus* ALE showed moderate decrees at all tested concentrations which confirms that the green ZnO NPs possess high toxicity against *S. aureus* bacteria rather than *C. citratus* ALE. On the contrary, *P. aeruginosa* displayed resistance towards both biosynthesized ZnO NPs and the ALE of *C. citratus*. Furthermore, the highest (%) inhibition of bacterial growth was noted for *S. aureus* at 200 µg/mL (94.66%), followed by 100 µg/mL (88.50%) while the lowest percentage of inhibition was detected at a concentration of 50 µg/mL (77.35%) and 25 µg/mL (65.74%), respectively, compared to control (0.0%), amoxicillin (40.20%) and the ALE of *C. citratus*, with 44.2% (at 200 µg/mL), 39.5% (at 100 µg/mL), 33.1% (at 50 µg/mL) and 0.0% (at 25 µg/mL), respectively.

It was evident from the results obtained that G(+)-bacterial strain was more susceptible to biosynthesized ZnO NPs than G(−)-bacterial strain. Our results are

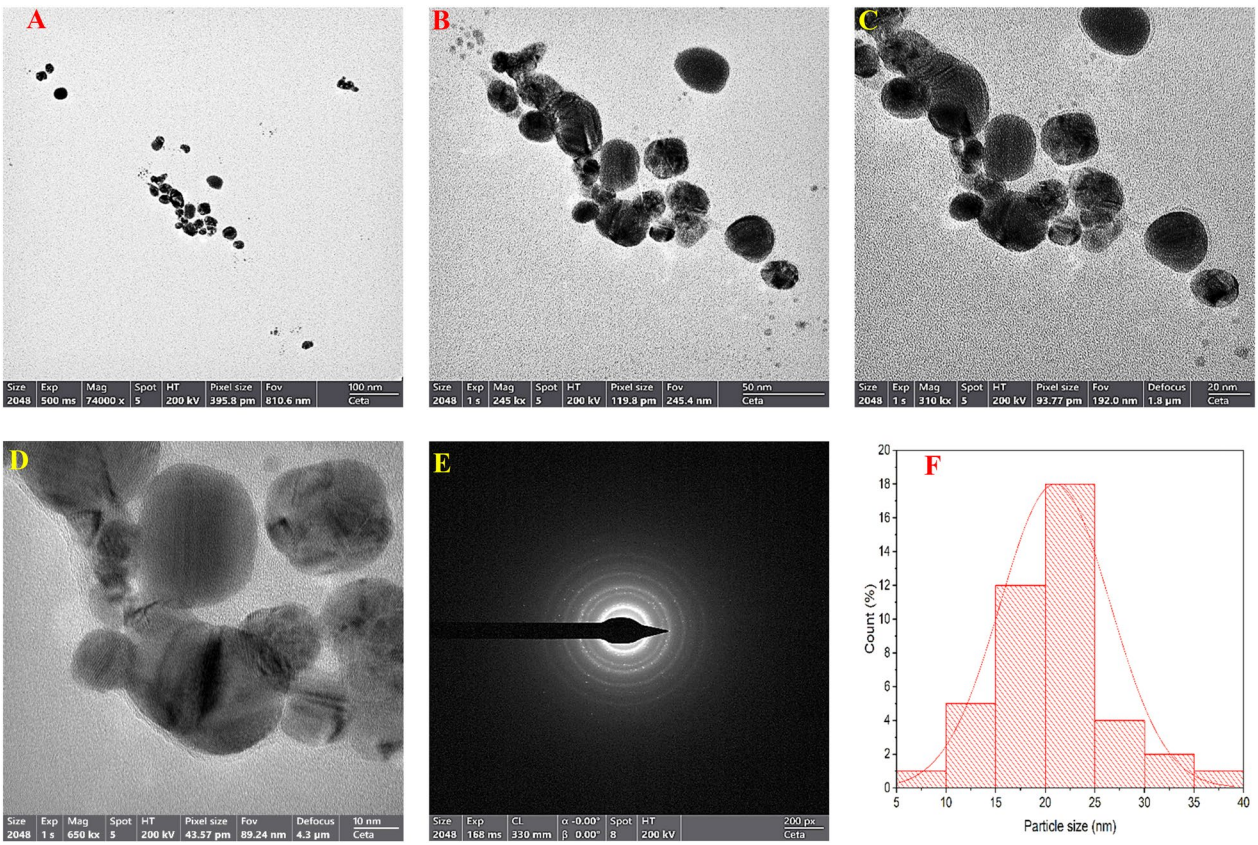

Fig. 10 **A**-**D** HR-TEM image of ZnO NPs biosynthesized using *C. citratus* ALE; **E** SAED pattern and **F** histogram displaying particle size distribution

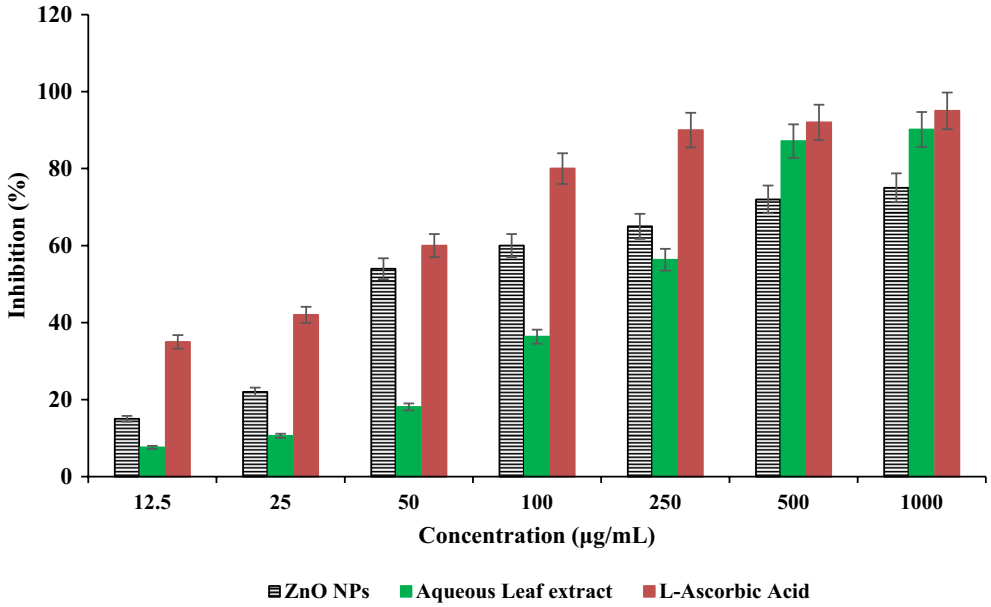

Fig. 11 Antioxidant activity of biosynthesized ZnO NPs, ALE of *C. citratus* and L-ascorbic acid (standard). The results mentioned are expressed as mean ± SD ($n = 3$)

more consistent with Ahmad et al. [93], Shinde et al. [94], Xie et al. [95] and Huang et al. [93–96] who found that as ZnO NP concentration increases, the effect on G(+)-bacterial strains becomes more pronounced. We observed the MIC and MBC values of biosynthesized ZnO NPs against *S. aureus* were 100 µg/mL and 200 µg/mL, respectively. Our findings are agreeing with earlier studies by Bala et al. [97], Bhuyan et al. [98] and Ahmad et al. [93] who showed that ZnO NPs synthesized via green routes against *S. aureus* had MIC and MBC at concentrations of 100 and 250 µg/mL, respectively.

The following mechanism may be used to explain how ZnO NPs produced via the green route have an antibacterial effect, which involves (1) the release of reactive oxygen species (ROS) (i.e. $O_2^{\bullet -2}$ (peroxide) and $OH^{\bullet}$ (hydroxyl radical), which causes oxidative stress, disruption of cell membrane, damage of DNA and eventually leads to cell death [99, 100]; (2) the dissolution of ZnO NPs into zinc ions (Zn^{2+}), which interact with the cell membrane of bacteria, nucleic acid, protein and cytoplasm, thus destroying the cellular integrity and causing bacterial cell death [101]; and (3) direct electrostatic interactions between ZnO NPs and bacterial cell membranes that result in plasma membrane disruption and intracellular component leaking [102–104] (Fig. 14). According to the aforementioned findings, it can be concluded that the inhibition of bacterial growth demonstrated by ZnO NPs displayed that they possessed strong antibacterial efficiency. This excellent antibacterial effect of biosynthesized ZnO NPs is due to the larger surface area of smaller NPs in size and possible mechanism mentioned above.

Antifungal activity

The major reason for significant economic loss during the post-harvest handling of fruits and grains is the growth of fungal pathogens (FP) in plants. Since fungi have gained resistance to several common fungicides, including dicarboximides and benzimidazoles [105], it is challenging to control the fungus development using organic substrate. A 20–30% reduction in crop output due to the fungus *Aspergillus* species infection of plants can be prevented by using different metal NPs because they have a potent antifungal impact on specific fungi [106]. *Aspergillus* species infections have been found, and they pose a serious threat to agricultural productivity losses.

According to the literature review, there is little research on the antifungal activity (AFA) of ZnO NPs. The AFA of ZnO NPs was examined by the poison food technique (PFT). This study is the first time to explore the effect of ZnO NPs as AFA against the important plant pathogenic fungus *A. niger*-mediated ALE of *C. citratus*.

ZnO NPs showed substantial antifungal efficacy against the phytopathogenic fungus *A. niger* (Fig. 15 and Table 4). Several ZnO NPs concentrations (25, 50, 100, 150, 200, 250, 500, 1000 and 2000 µg/mL) employed in the PDA medium had a dose-dependent influence on reducing the radial mycelial growth (RMG) of *A. niger*. It is clearly evident from the results in Fig. 15 and Table 4 that all

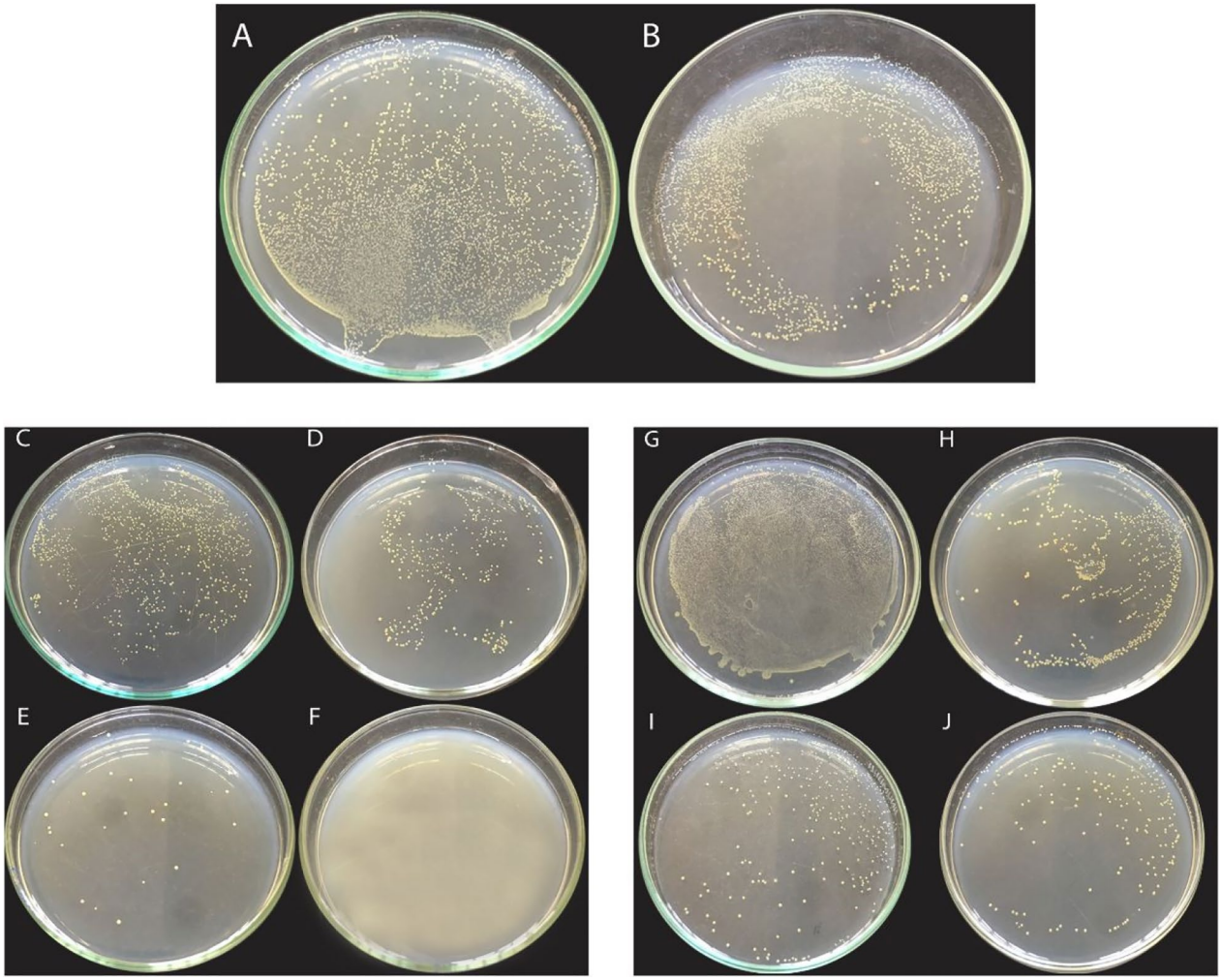

Fig. 12 The viability of bacterial cells with ZnO NPs. *S. aureus* with **A** control (0 ug/ml); **B** antibiotic (amoxicillin, 25 µg/mL); **C** ZnO NPs at 25 µg/mL; **D** ZnO NPs at 50 µg/mL; **E** ZnO NPs at 100 µg/mL; **F** ZnO NPs at 200 µg/mL; **G** ALE at 25 µg/mL; **H** ALE at 50 µg/mL; **I** ALE at 100 µg/mL; **J** ALE at 200 µg/mL cultured on agar plates. The findings mentioned are represented as mean ± SD ($n = 3$)

concentrations of ZnO NPs significantly decreased the fungal biomass in a concentration-dependent manner compared to the control (Fig. 15A). A maximum inhibition rate (IR) (95.13%) of mycelia growth was recorded at 2000 µg/mL (0.2% w/v, Fig. 15J) of ZnO NPs followed by 87.62% at 1000 µg/mL (0.1% w/v, Fig. 15I) concentration while the other concentrations (500–25 µg/mL, Fig. 15B–H) gave IR from 75.12 to 18.75% (Table 4).

Our results unequivocally show that ZnO NPs may be an effective antifungal agent against pathogenic fungi that can aid in preventing crop infection by not only *A. niger*, but also other species of Aspergillus and other closely related fungi (Table 4).

Anti-inflammatory activity

Inflammation or pain is a common phenomenon that is a reflective response of living tissues to a stimulus like infection, injury cells, etc. [107, 108]. Lysosome organelle lyses and releases their constituent enzymes during periods of inflammation, causing a number of diseases. The mechanism of action of nonsteroidal anti-inflammatory medications (NSAIDs) is either stabilizing lysosomal membranes or preventing the release of lysosomal enzymes [109]. Haemolysis and haemoglobin oxidation occur when RBCs are subjected to hazardous substances including heat, chemical agents, i.e. methyl salicylate, phenylhydrazine, bacterial infection, hypotonic medium, or any of these [110]. Due to the similarity between the membranes of hRBCs and lysosomes, the hypotonicity-induced RBCs membrane lysis was

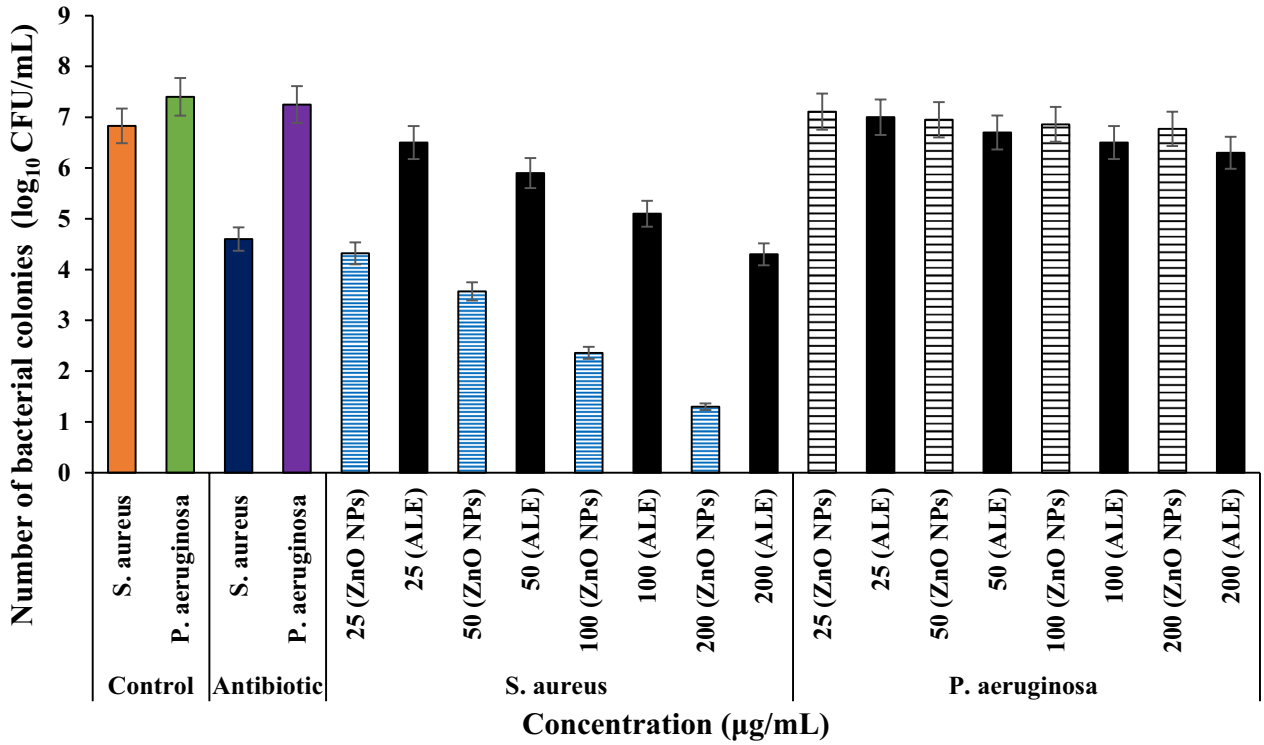

Fig. 13 The number of *S. aureus (ATCC 8095) and P. aeruginosa (ATCC10662)* colonies expressed as the logarithm (log) of the CFU grown on the agar plates treated with various concentrations of ZnO NPs compared with the control of bacteria (without ZnO NPs) and amoxicillin as a (+) control

used to examine the mechanism behind ZnO NPs and *C. citratus* ALE anti-inflammatory activity [109]. The present findings (Fig. 16) found that the ALE of *C. citratus* and biosynthesized ZnO NPs possess a concentration-dependent anti-inflammatory effect, with the increasing concentrations of both *C. citratus* ALE and ZnO NPs, the percentage of protection was found to be increased. Thus, the results clearly reveal that biosynthesized ZnO NPs are better anti-inflammatory effects than both the reference NSAID indomethacin and *C. citratus* ALE. The possible anti-inflammatory mechanisms used by ZnO NPs involve the release of zinc ions (Zn^{2+}) from the dissolution of ZnO NPs and subsequent blocking of the production of proinflammatory cytokines (such as interleukin-1, 1β and 13) and inhibit or suppress expression of the lipo-polysaccharide-induced cyclo-oxygenase gene to prevent the generation of prostaglandin-E2 and it is possible that ZnO NPs prevented the release of active inflammatory mediators (i.e. leukotrienes, chemokines, histamines, and cytokines) and haemolytic enzymes, which stabilized the RBC membrane.

In vitro *cytotoxicity effect*

The cytotoxicity of biosynthesized ZnO NPs and *C. citratus* ALE was evaluated on seven human cancer cell lines (i.e. H1299, MDA-MB-468, HNO97, HEK, HCT116, HuH7 and HEPG2) and normal cells (HSF) treated with four different concentrations (12.5, 25, 50 and 100 µg/mL, respectively, in case of ZnO NPs) and (62.5, 125, 250 and 500 µg/mL, respectively, in case of *C. citratus* ALE) for 48 h in comparison with doxorubicin (DOX) as a chemotherapeutic guiding drug by sulphorhodamine-B (SRB) assay which one of the most popular techniques is still in use for in vitro cytotoxicity screening. From the data represented in Fig. 17, there was a sharp decrease after 48 h in survival fraction following exposure to ZnO NPs at doses ranging from 12.5 to 100 µg/mL of all examined cells in a concentration-dependent manner. In contrast, the findings showed that there is a non-significant effect on normal cells (HSF) upon exposure to ZnO NPs up to 100 µg/mL. On the other hand, DOX displayed a cytotoxic effect on both cancer and normal cells.

According to our findings, the biosynthesized ZnO NPs have a promising anticancer potential, with inhibitory concentrations ranging from one cancer cell line to another and less cytotoxicity against normal cells, according to the in vitro cytotoxicity studies. Contrarily,

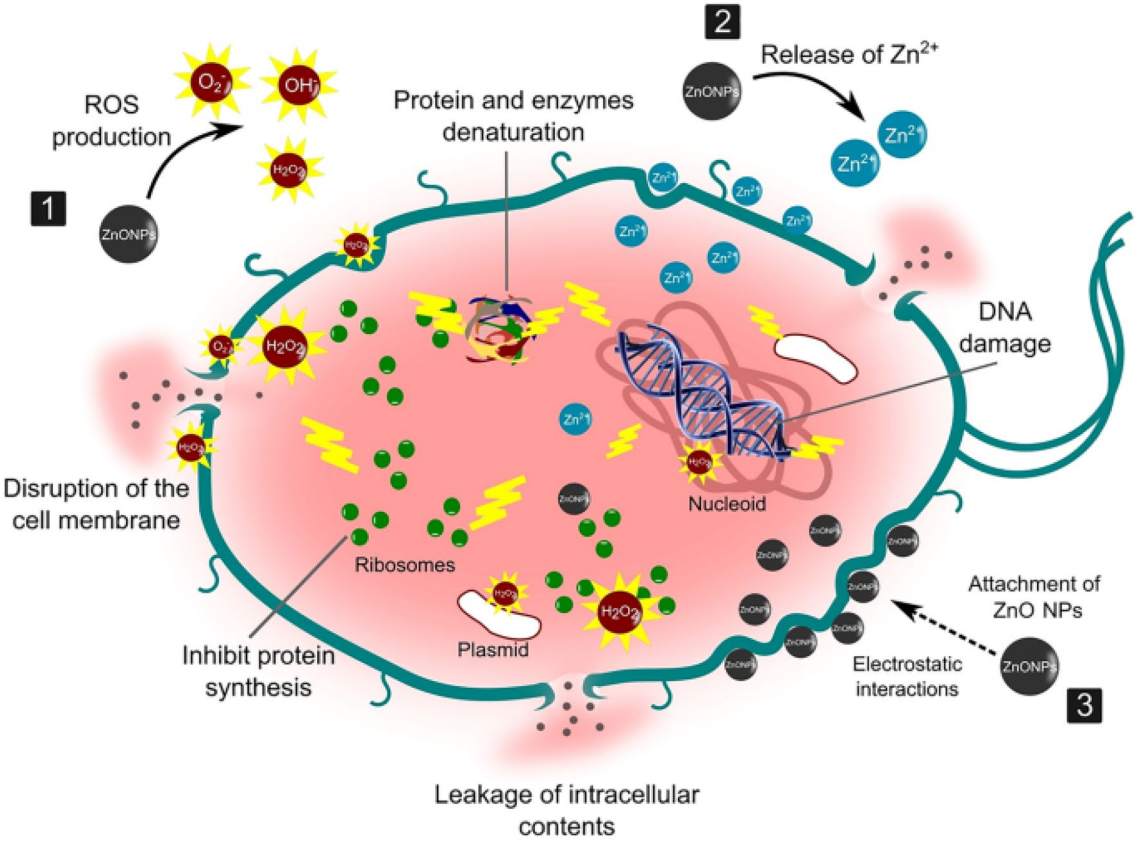

Fig. 14 Schematic representation of the antibacterial mechanism of ZnO NPs against the bacterial cells. (Reprinted from [104]; open access under CC BY.)

commercial chemotherapy (DOX) has a similar cytotoxic effect on both cancerous and normal cells. One of the biggest challenges with cancer chemotherapy at the moment is doxorubicin's inability to distinguish between

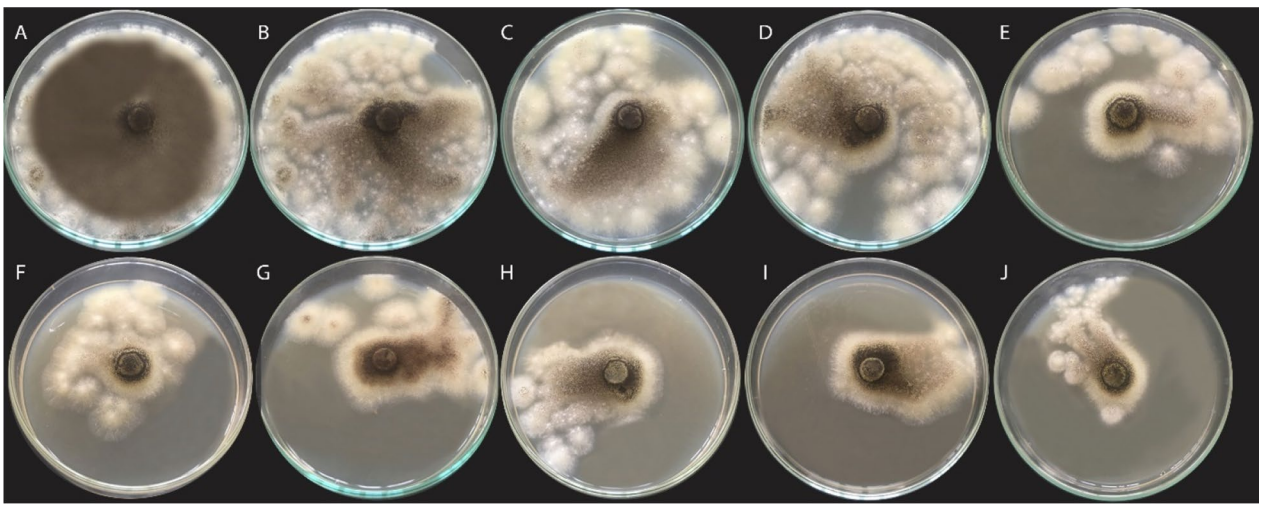

Fig. 15 Effect of biosynthesized ZnO NPs on mycelial growth of *A. niger* by PFT **A** Control (0 µg/mL); **B** 25 µg/mL; **C** 50 µg/mL; **D** 100 µg/mL; **E** 150 µg/mL; **F** 200 µg/mL; **G** 250 µg/mL; **H** 500 µg/mL; **I** 1000 µg/mL; and **J** 2000 µg/mL ZnO NPs. The findings mentioned are represented as mean ± SD ($n = 3$)

Table 4 Effect of different concentrations of ZnO NPs on percentage inhibition of mycelial growth (MG) of phytopathogenic fungus *A. niger*

Treatments (µg/mL)	% Inhibition MG[a]
ZnO NPs	
25	10.15 ± 3.0 [g]
50	18.75 ± 2.1 [f]
100	22.50 ± 1.0 [f]
150	60.00 ± 0.6 [e]
200	62.50 ± 0.9 [e]
250	69.37 ± 0.5 [d]
500	75.12 ± 0.7 [c]
1000	87.62 ± 0.3 [b]
2000	95.13 ± 0.1 [a]
Control[b]	00.00 ± 0.0 [h]

[a] Each value is the average of three replicates. Mean ± SD followed by the different superscript letters (a-g) in a column of each concentration is a significant difference at $p < 0.05$ and the % inhibition of MG was measured compared to the growth of the control (0%). [b]Control without NPs

cancer and normal cells. The biosynthesized ZnO NPs possess selective killing abilities that may be a result of the production of ROS [111]. Our results are consistent with earlier studies by Selim et al. [112], who reported that ZnO NPs prepared using an ALE of *Deverra tortuosa* had selective cytotoxicity on A549 and Caco-2 cancer cells while having lower cytotoxicity on normal W138 cells.

The IC_{50} values of ZnO NPs (Fig. 17) displayed that the concentration needed to cause 50% cell death was 20 ± 0.62, 26 ± 0.58, 27 ± 0.43, 46 ± 0.61, 54 ± 0.76, 60 ± 0.59 and 90 ± 0.66 µg/mL for H1299, MDA-MB-468, HNO97, HEK, HCT116, HuH7 and HEPG2, respectively, which significantly much lower than that of *C. citratus* ALE (Fig. 17). Also, ZnO NPs exhibited no IC_{50} value in normal cells (HSF) till 100 µg/mL, indicating that the cytotoxicity of ZnO NPs is sufficient. On the other hand, the cancer cell lines were not affected by the ALE of *C. citratus* at any concentrations tested, thus there no IC_{50} values were determined for it.

Consistent with our results, Hassan et al. [113] reported that IC_{50} value for green ZnO NPs (average particle size = 35 nm) on cancer cell lines i.e. Hep G2, PC-3 and A-549 were 34.67, 36.31 and 21.38 µg/mL, respectively. Our results were also confirmed by another study by Senthilkumar et al. [114], who revealed that the IC_{50} value for biosynthesized ZnO NPs on the MC3t3-EI cancer cell line was 41.29 µg/mL. Furthermore, Manosroi et al. [115] reported that samples with IC_{50} value less than 0.125 mg/mL might be a promising candidate for further development into a cancer therapeutic agent,

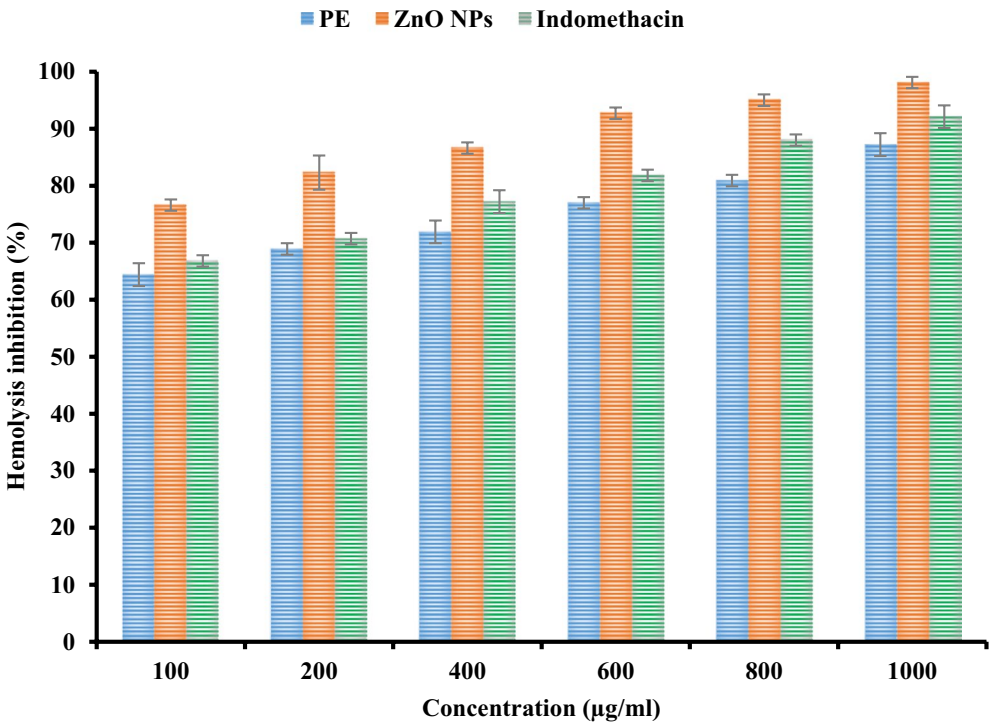

Fig. 16 Anti-inflammatory activity of *C. citratus* ALE, biosynthesized ZnO NPs and indomethacin as a standard. Each bar is expressed as the mean ± standard error of the mean ($n = 3$)

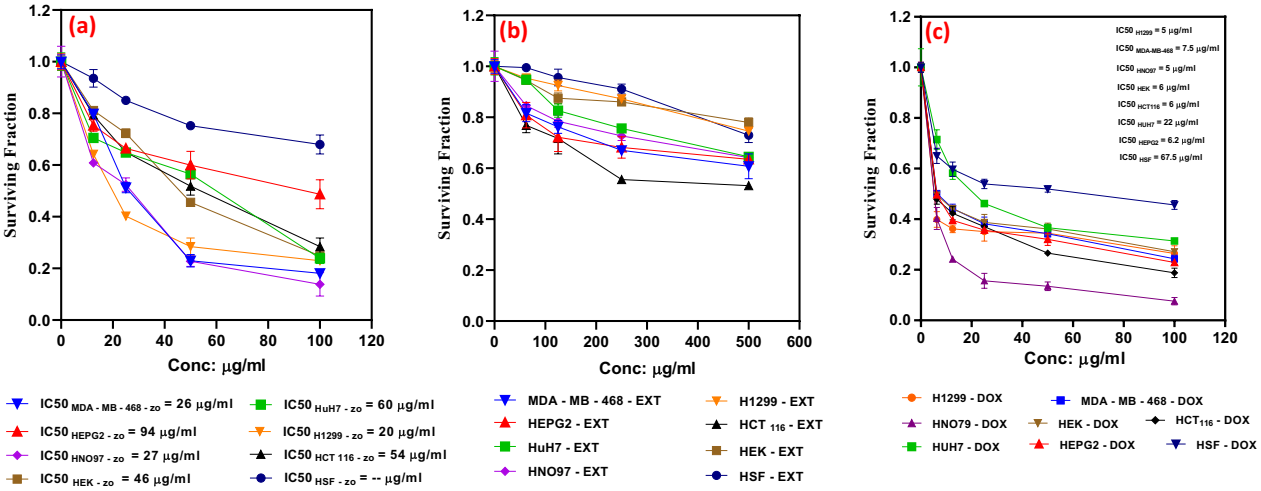

Fig. 17 IC_{50} values of various human cancer cell lines treated with biosynthesized **a** ZnO NPs, **b** *C. citratus* ALE and **c** doxorubicin by SRB assay at different concentration. The data mentioned are represented as mean ± SD ($n = 3$)

while samples having an IC_{50} values between 0.125 and 5.0 mg/mL had a moderate potential to be developed into a cancer therapeutic agent. In our study, biosynthesized ZnO NPs possibly considered as a strong potential source for lung, breast, oral, kidney, colon and liver cancer (20 ± 0.62, 26 ± 0.58, 27 ± 0.43, 46 ± 0.61, 54 ± 0.76, 60 ± 0.59 and 90 ± 0.66 µg/mL, respectively). Additionally, there was no information on the cytotoxic effects of biosynthesized ZnO NPs prepared by *C. citratus* ALE. One of the possible mechanisms for ZnO NPs cytotoxicity against cancer cells is their (1) dissolution to Zn^{2+} ions, which leads to oxidative stress (through ROS generation) and subsequent cell death in cancer cells and (2) the generation of significantly greater amounts of ROS in cancer cells than in healthy (normal) cells, which leads to mitochondrial dysfunction and stimulates the intrinsic mitochondrial apoptotic pathway [116]. Additionally, an excess of ROS overproduction can cause autophagic/mitophagic cell death as well as promote oxidative DNA damage and mitotic death (Fig. 18) [117, 118].

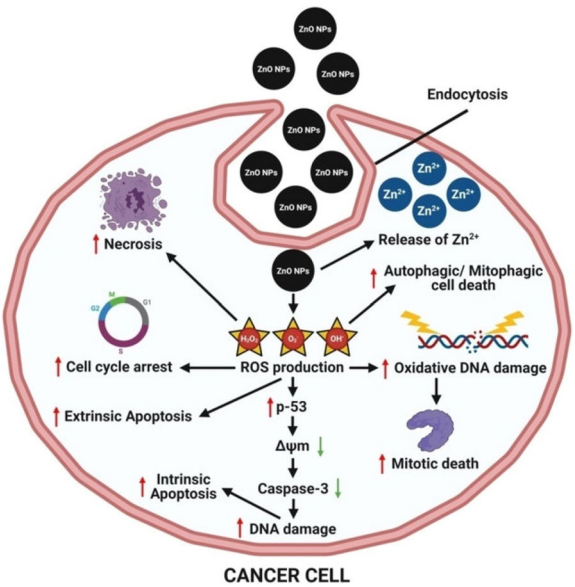

Fig. 18 Proposed anticancer mechanism of ZnO NPs biosynthesized using *C. citratus* ALE. (Reprinted from [103]; open access under CC BY.)

Conclusion

This research presents a straightforward, cost-effective, easy, safe and environmentally friendly approach to biosynthesized ZnO NPs on a broad scale for the first time via a green route by ALE of *C. citratus*. The crystalline nature of the biosynthesized ZnO NPs was confirmed by XRD analysis. Several vibrational bands have been identified by FTIR, and they were related to the components present in the corresponding extracts and ZnO NPs. Both the observation of a colour change and a peak at 370 nm in UV–Vis spectroscopy provided evidence that ZnO NPs were being formed. The particle size and potential stability of the dispersion solution containing ZnO NPs are confirmed by DLS investigations. The spherical shape of biosynthesized ZnO NPs with an average mean size of 21 nm was confirmed by HR-TEM analysis. The HPLC profile of *C. citratus* ALE revealed 16 polyphenolic compounds that are maybe responsible for the bio-reduction and formation of NPs. Biosynthesized ZnO NPs displayed a potential antioxidant effect with an IC_{50} value of 45.67 ± 0.1 µg/mL and superior anti-inflammatory activity through stabilization of the hRBCs

MSA in vitro model. Furthermore, the biosynthesized ZnO nanoparticles showed significant antibacterial activity against both G(+) *S. aureus*, and G(−) *P. aeruginosa* bacteria as well as excellent fungicidal activity towards plant pathogenic fungus *Aspergillus niger*, respectively. In addition, ZnO nanoparticles had a remarkable selective cytotoxic effect against seven human cancer cell lines (i.e. H1299, MDA-MB-468, HNO97, HEK, HCT116, HuH7 and HEPG2) and less cytotoxicity against normal cells under in vitro conditions. This effect may be linked to the upregulation of proapoptotic proteins and the downregulation of antiapoptotic proteins. Our data suggested that the currently adopted approach for synthesizing stable ZnO NPs using the ALE of *C. citratus* provides a satisfying safer, and cheaper alternative over other methods and could be of great prominence in biomedical research, drug delivery process and has a promising effect against biological systems-related applications.

Author contributions
Designed the experiment: ASA, NAM and YMD; prepared the samples: ASA, NAM, AMHAM and MS; methodology: ASA, NAM, AMHAM and MS; biosynthesis and characterizations: ASA and NAM; performed the experiments: ASA, NAM, AMHAM and MS; data analysed and software: ASA; wrote the paper: ASA and AMHAM; review and checked: ASA, AMHAM and YMD. All authors have read and approved the final version of the manuscript.

Funding
Open access funding provided by The Science, Technology & Innovation Funding Authority (STDF) in cooperation with The Egyptian Knowledge Bank (EKB).

Availability of data and materials
All data are presented within the article.

Declarations

Ethics approval and consent to participate
Not applicable.

Consent for publication
Not applicable.

Competing interests
The authors have no competing interests.

Author details
[1]Department of Biochemistry, Faculty of Agriculture, Fayoum University, Fayoum 63514, Egypt. [2]Department of Agricultural Microbiology, Faculty of Agriculture, Fayoum University, Fayoum 63514, Egypt. [3]Pharmacology Unit, Cancer Biology Department, National Cancer Institute, Cairo University, Giza, Egypt.

Received: 22 March 2023 Accepted: 16 June 2023
Published online: 20 July 2023

References

1. Nikzamir M, Akbarzadeh A, Panahi Y. An overview on nanoparticles used in biomedicine and their cytotoxicity. J Drug Deliv Sci Technol. 2021;61:102316.
2. Bayda S, Adeel M, Tuccinardi T, Cordani M, Rizzolio F. The history of nanoscience and nanotechnology: from chemical–physical applications to nanomedicine. Molecules. 2019;25:112.
3. Hulla JE, Sahu SC, Hayes AW. Nanotechnology: history and future. Hum Exp Toxicol. 2015;34:1318–21.
4. Sharma A, Vijayakumar PS, Prabhakar EPK, Kumar R. Nanotechnology applications for food safety and quality monitoring. Amsterdam: Elsevier Science & Technology; 2022.
5. Muhammad W, Khan MA, Nazir M, Siddiquah A, Mushtaq S, Hashmi SS, et al. *Papaver somniferum* L. mediated novel bioinspired lead oxide (PbO) and iron oxide (Fe2O3) nanoparticles: In-vitro biological applications, biocompatibility and their potential towards HepG2 cell line. Mater Sci Eng: C. 2019;103:109740.
6. Kaur S, Roy A. Bioremediation of heavy metals from wastewater using nanomaterials. Environ Dev Sustain. 2021;23:9617–40.
7. Roy A. Plant derived silver nanoparticles and their therapeutic applications. Curr Pharm Biotechnol. 2021;22:1834–47.
8. Savunthari KV, Arunagiri D, Shanmugam S, Ganesan S, Arasu MV, Al-Dhabi NA, et al. Green synthesis of lignin nanorods/g-C3N4 nanocomposite materials for efficient photocatalytic degradation of triclosan in environmental water. Chemosphere. 2021;272:129801.
9. Geonmonond RS, Silva AGMDA, Camargo PHC. Controlled synthesis of noble metal nanomaterials: motivation, principles, and opportunities in nanocatalysis. An Acad Bras Cienc. 2018;90:719–44.
10. Qiao X, He J, Yang R, Li Y, Chen G, Xiao S, et al. Recent advances in nanomaterial-based sensing for food safety analysis. Processes. 2022;10:2576.
11. Yang M, Li J, Gu P, Fan X. The application of nanoparticles in cancer immunotherapy: targeting tumor microenvironment. Bioact Mater. 2021;6:1973–87.
12. Pandit C, Roy A, Ghotekar S, Khusro A, Islam MN, Bin ET, et al. Biological agents for synthesis of nanoparticles and their applications. J King Saud Univ-Sci. 2022;34:101869.
13. Ramanathan S, Gopinath SCB, Arshad MKM, Poopalan P, Perumal V. Nanoparticle synthetic methods: strength and limitations nanoparticles in analytical and medical devices. Amsterdam: Elsevier; 2021. p. 31–43.
14. Khan N, Ali S, Latif S, Mehmood A. Biological synthesis of nanoparticles and their applications in sustainable agriculture production. Nat Sci. 2022;14:226–34.
15. Malhotra SPK, Alghuthaymi MA. Biomolecule-assisted biogenic synthesis of metallic nanoparticles agri-waste and microbes for production of sustainable nanomaterials. Amsterdam: Elsevier; 2022. p. 139–63.
16. Mohammadlou M, Maghsoudi H, Jafarizadeh-Malmiri H. A review on green silver nanoparticles based on plants: synthesis, potential applications and eco-friendly approach. Int Food Res J. 2016;23:446.
17. Devi HS, Boda MA, Shah MA, Parveen S, Wani AH. Green synthesis of iron oxide nanoparticles using *Platanus* orientalis leaf extract for antifungal activity. Green Process Synth. 2019;8:38–45.
18. Alsammarraie FK, Wang W, Zhou P, Mustapha A, Lin M. Green synthesis of silver nanoparticles using turmeric extracts and investigation of their antibacterial activities. Coll Surf B Biointerfaces. 2018;171:398–405.
19. Ahmed S, Chaudhry SA, Ikram S. A review on biogenic synthesis of ZnO nanoparticles using plant extracts and microbes: a prospect towards green chemistry. J Photochem Photobiol B. 2017;166:272–84.
20. Singh P, Kim Y-J, Zhang D, Yang D-C. Biological synthesis of nanoparticles from plants and microorganisms. Trends Biotechnol. 2016;34:588–99.
21. Duan H, Wang D, Li Y. Green chemistry for nanoparticle synthesis. Chem Soc Rev. 2015;44:5778–92.
22. Samuel MS, Ravikumar M, John JA, Selvarajan E, Patel H, Chander PS, et al. A review on green synthesis of nanoparticles and their diverse biomedical and environmental applications. Catalysts. 2022;12:459.
23. Can M. Green gold nanoparticles from plant-derived materials: an overview of the reaction synthesis types, conditions, and applications. Rev Chem Eng. 2020;36:859–77.
24. Makarov VV, Love AJ, Sinitsyna OV, Makarova SS, Yaminsky IV, Taliansky ME, et al. "Green" nanotechnologies: synthesis of metal nanoparticles using plants. Acta Naturae. 2014;6:35–44.
25. Rajendran SP, Sengodan K. Synthesis and characterization of zinc oxide and iron oxide nanoparticles using *Sesbania* grandiflora leaf extract as reducing agent. J Nanosci. 2017;2017:1.

26. Ahmed S, Ahmad M, Swami BL, Ikram S. A review on plants extract mediated synthesis of silver nanoparticles for antimicrobial applications: a green expertise. J Adv Res. 2016;7:17–28.
27. Rajan R, Chandran K, Harper SL, Yun S-I, Kalaichelvan PT. Plant extract synthesized silver nanoparticles: an ongoing source of novel biocompatible materials. Ind Crops Prod. 2015;70:356–73.
28. Khalafi T, Buazar F, Ghanemi K. Phycosynthesis and enhanced photocatalytic activity of zinc oxide nanoparticles toward organosulfur pollutants. Sci Rep. 2019;9:1–10.
29. Rastogi A, Zivcak M, Sytar O, Kalaji HM, He X, Mbarki S, et al. Impact of metal and metal oxide nanoparticles on plant: a critical review. Front Chem. 2017;5:78.
30. Sabir S, Arshad M, Chaudhari SK. Zinc oxide nanoparticles for revolutionizing agriculture: synthesis and applications. Sci World J. 2014;2014:1.
31. Fouda A, Saad EL, Salem SS, Shaheen TI. *In-vitro* cytotoxicity, antibacterial, and UV protection properties of the biosynthesized zinc oxide nanoparticles for medical textile applications. Microb Pathog. 2018;125:252–61.
32. Mirzaei H, Darroudi M. Zinc oxide nanoparticles: biological synthesis and biomedical applications. Ceram Int. 2017;43:907–14.
33. Sushma NJ, Mahitha B, Mallikarjuna K, Raju BDP. Bio-inspired ZnO nanoparticles from *Ocimum tenuiflorum* and their in vitro antioxidant activity. Appl Phys A. 2016;122:1–10.
34. Kołodziejczak-Radzimska A, Jesionowski T. Zinc oxide—from synthesis to application: a review. Materials. 2014;7:2833–81.
35. Abedini M, Shariatmadari F, Karimi Torshizi MA, Ahmadi H. Effects of zinc oxide nanoparticles on the egg quality, immune response, zinc retention, and blood parameters of laying hens in the late phase of production. J Anim Physiol Anim Nutr. 2018;102:736–45.
36. Yeşil Y, Akalin E. Comparative morphological and anatomical characteristics of the species known as lemongrass (limonotu): Melissa officinalis L., *Cymbopogon citratus* (DC) Stapf. and *Aloysia citriodora* Palau. J Fac Pharm Istanb Univ. 2015;45:29–37.
37. Ojo OO, Kabutu FR, Bello M, Babayo U. Inhibition of paracetamol-induced oxidative stress in rats by extracts of lemongrass (*Cymbopogon citratus*) and green tea (*Camellia sinensis*) in rats. Afr J Biotechnol. 2006;5.
38. Sahal G, Woerdenbag HJ, Hinrichs WLJ, Visser A, Tepper PG, Quax WJ, et al. Antifungal and biofilm inhibitory effect of *Cymbopogon citratus* (lemongrass) essential oil on biofilm forming by Candida tropicalis isolates; an *in vitro* study. J Ethnopharmacol. 2020;246:112188.
39. Pinto ZT, Sánchez FF, dos Santos AR, Amaral ACF, Ferreira JLP, Escalona-Arranz JC, et al. Chemical composition and insecticidal activity of *Cymbopogon citratus* essential oil from Cuba and Brazil against housefly. Rev Bras Parasitol Vet. 2015;24:36–44.
40. Kpoviessi S, Bero J, Agbani P, Gbaguidi F, Kpadonou-Kpoviessi B, Sinsin B, et al. Chemical composition, cytotoxicity and in vitro antitrypanosomal and antiplasmodial activity of the essential oils of four Cymbopogon species from Benin. J Ethnopharmacol. 2014;151:652–9.
41. Vickers NJ. Animal communication: when i'm calling you, will you answer too? Curr Biol. 2017;27:R713–5.
42. Bieski IGC, Leonti M, Arnason JT, Ferrier J, Rapinski M, Violante IMP, et al. Ethnobotanical study of medicinal plants by population of valley of Juruena region, legal Amazon, Mato Grosso. Brazil J Ethnopharmacol. 2015;173:383–423.
43. Kiani HS, Ali A, Zahra S, Hassan ZU, Kubra KT, Azam M, et al. Phytochemical composition and pharmacological potential of Lemongrass (*Cymbopogon*) and Impact on gut microbiota. AppliedChem. 2022;2:229–46.
44. Kassahun T, Girma B, Joshi RK, Sisay B, Tesfaye K, Taye S, et al. Ethnobotany, traditional use, phytochemistry and pharmacology of *Cymbopogon citratus*: review article. Int J Herb Med. 2020;8:80–7.
45. Umar M, Mohammed I, Oko J, Tafinta I, Aliko A, Jobbi D. Phytochemical Analysis and antimicrobial effect of lemon grass (*Cymbopogon citratus*) obtained from Zaria, Kaduna State, Nigeria. J Complement Altern Med Res. 2016;1:1–8.
46. Brand-Williams W, Cuvelier ME, Berset C. Use of a free radical method to evaluate antioxidant activity. LWT—Food Sci Technol. 1995. https://doi.org/10.1016/S0023-6438(95)80008-5.
47. Trabelsi I, Ayadi D, Bejar W, Bejar S, Chouayekh H, Ben SR. Effects of *Lactobacillus plantarum* immobilization in alginate coated with chitosan and gelatin on antibacterial activity. Int J Biol Macromol. 2014;64:84–9.
48. Soylu S, Yigitbas H, Soylu EM, Kurt Ş. Antifungal effects of essential oils from oregano and fennel on *Sclerotinia sclerotiorum*. J Appl Microbiol. 2007;103:1021–30.
49. Skehan P, Storeng R, Scudiero D, Monks A, Mcmahon J, Vistica D, et al. New colorimetric cytotoxicity assay for anticancer-drug screening. J Natl Cancer Inst. 1990;82:1107–12.
50. Sharma D, Kanchi S, Bisetty K. Biogenic synthesis of nanoparticles: a review. Arab J Chem. 2019;12:3576–600.
51. Saranya KS, Vellora Thekkae Padil V, Senan C, Pilankatta R, Saranya K, George B, et al. Green synthesis of high temperature stable anatase titanium dioxide nanoparticles using Gum Kondagogu: characterization and solar driven photocatalytic degradation of organic dye. Nanomaterials. 2018;8:1002.
52. Kumar H, Rani R. Structural and optical characterization of ZnO nanoparticles synthesized by microemulsion route. Int Lett Chem Phys Astron. 2013;14:26–36.
53. Kim J, Rheem Y, Yoo B, Chong Y, Bozhilov KN, Kim D, et al. Peptide-mediated shape-and size-tunable synthesis of gold nanostructures. Acta Biomater. 2010;6:2681–9.
54. Si S, Mandal TK. Tryptophan-based peptides to synthesize gold and silver nanoparticles: a mechanistic and kinetic study. Chem—A Eur J. 2007;13:3160–8.
55. Glusker J, Katz A, Bock C. Metal ions in biological systems. Rigaku J. 1999;16:8–16.
56. Zak AK, Majid WHA, Mahmoudian MR, Darroudi M, Yousefi R. Starch-stabilized synthesis of ZnO nanopowders at low temperature and optical properties study. Adv Powder Technol. 2013;24:618–24.
57. Zak AK, Yousefi R, Abd Majid WH, Muhamad MR. Facile synthesis and X-ray peak broadening studies of Zn1− xMgxO nanoparticles. Ceram Int. 2012;38:2059–64.
58. Kayani ZN, Saleemi F, Batool I. Synthesis and characterization of ZnO nanoparticles. Mater Today Proc. 2015;2:5619–21.
59. Badran M. Formulation and *in vitro* evaluation of flufenamic acid loaded deformable liposomes for improved skin delivery. Dig J Nanomater Biostruct. 2014;9.
60. Putri DCA, Dwiastuti R, Marchaban M, Nugroho AK. Optimization of mixing temperature and sonication duration in liposome preparation. J Pharm Sci Community. 2017;14:79–85.
61. Meléndrez MF, Cárdenas G, Arbiol J. Synthesis and characterization of gallium colloidal nanoparticles. J Colloid Interface Sci. 2010;346:279–87.
62. García AB, Cuesta A, Montes-Morán MA, Martínez-Alonso A, Tascón JMD. Zeta potential as a tool to characterize plasma oxidation of carbon fibers. J Coll Interface Sci. 1997;192:363–7.
63. Abdelbaky AS, Abd El-Mageed TA, Babalghith AO, Selim S, Mohamed AMHA. Green synthesis and characterization of ZnO nanoparticles using pelargonium *odoratissimum* (L.) aqueous leaf extract and their antioxidant antibacterial and anti-inflammatory activities. Antioxidants. 2022;11:1444.
64. Jafarirad S, Mehrabi M, Divband B, Kosari-Nasab M. Biofabrication of zinc oxide nanoparticles using fruit extract of *Rosa canina* and their toxic potential against bacteria: a mechanistic approach. Mater Sci Eng, C. 2016;59:296–302.
65. Awwad AM, Albiss B, Ahmad AL. Green synthesis, characterization and optical properties of zinc oxide nanosheets using Olea europea leaf extract. Adv Mater Lett. 2014;5:520–4.
66. Narath S, Koroth SK, Shankar SS, George B, Mutta V, Wacławek S, et al. *Cinnamomum tamala* leaf extract stabilized zinc oxide nanoparticles: a promising photocatalyst for methylene blue degradation. Nanomaterials. 2021;11:1558.
67. El-Belely EF, Farag MMS, Said HA, Amin AS, Azab E, Gobouri AA, et al. Green synthesis of zinc oxide nanoparticles (ZnO-NPs) using *Arthrospira platensis* (Class: Cyanophyceae) and evaluation of their biomedical activities. Nanomaterials. 2021;11:95.
68. Jabs A. Determination of secondary structure in proteins by Fourier transform infrared spectroscopy (FTIR). Jena Library of Biologica Macromol. 2005

69. Nagarajan S, Arumugam KK. Extracellular synthesis of zinc oxide nanoparticle using seaweeds of gulf of Mannar India. J Nanobiotechnol. 2013;11:1–11.
70. Sundrarajan M, Ambika S, Bharathi K. Plant-extract mediated synthesis of ZnO nanoparticles using Pongamia pinnata and their activity against pathogenic bacteria. Adv Powder Technol. 2015;26:1294–9.
71. Stan M, Popa A, Toloman D, Silipas T-D, Vodnar DC. Antibacterial and antioxidant activities of ZnO nanoparticles synthesized using extracts of Allium sativum, *Rosmarinus* officinalis and *Ocimum basilicum*. Acta Metallurgica Sinica (English Letters). 2016;29:228–36.
72. Senthilkumar N, Nandhakumar E, Priya P, Soni D, Vimalan M, Potheher IV. Synthesis of ZnO nanoparticles using leaf extract of Tectona grandis (L.) and their anti-bacterial, anti-arthritic, anti-oxidant and in vitro cytotoxicity activities. New J Chem. 2017;41:10347–56.
73. Ali K, Dwivedi S, Azam A, Saquib Q, Al-Said MS, Alkhedhairy AA, et al. Aloe vera extract functionalized zinc oxide nanoparticles as nanoantibiotics against multi-drug resistant clinical bacterial isolates. J Coll Interface Sci. 2016;472:145–56.
74. Yuvakkumar R, Suresh J, Saravanakumar B, Nathanael AJ, Hong SI, Rajendran V. Rambutan peels promoted biomimetic synthesis of bioinspired zinc oxide nanochains for biomedical applications. Spectrochim Acta A Mol Biomol Spectrosc. 2015;137:250–8.
75. Zhang G, Shen X, Yang Y. Facile synthesis of monodisperse porous ZnO spheres by a soluble starch-assisted method and their photocatalytic activity. J Phys Chem C. 2011;115:7145–52.
76. Fakhari S, Jamzad M, Kabiri FH. Green synthesis of zinc oxide nanoparticles: a comparison. Green Chem Lett Rev. 2019;12:19–24.
77. Buazar F, Bavi M, Kroushawi F, Halvani M, Khaledi-Nasab A, Hossieni SA. Potato extract as reducing agent and stabiliser in a facile green one-step synthesis of ZnO nanoparticles. J Exp Nanosci. 2016;11:175–84.
78. Abdelbaky AS, Mohamed AMHA, Alharthi SS. Antioxidant and antimicrobial evaluation and chemical investigation of *Rosa gallica var. aegyptiaca* leaf extracts. Molecules. 2021;26:6498.
79. Palafox-Carlos H, Yahia EM, González-Aguilar GA. Identification and quantification of major phenolic compounds from mango (Mangifera indica, cv. Ataulfo) fruit by HPLC–DAD–MS/MS-ESI and their individual contribution to the antioxidant activity during ripening. Food Chem. 2012;135:105–11.
80. Yuvakkumar R, Suresh J, Nathanael AJ, Sundrarajan M, Hong SI. Novel green synthetic strategy to prepare ZnO nanocrystals using rambutan (*Nephelium lappaceum* L.) peel extract and its antibacterial applications. Mater Sci Eng: C. 2014;41:17–27.
81. Alamdari S, Sasani Ghamsari M, Lee C, Han W, Park H-H, Tafreshi MJ, et al. Preparation and characterization of zinc oxide nanoparticles using leaf extract of *Sambucus ebulus*. Appl Sci. 2020;10:3620.
82. Talam S, Karumuri SR, Gunnam N. Synthesis, characterization, and spectroscopic properties of ZnO nanoparticles. ISRN Nanotechnol. 2012;2012:1–6.
83. Kajbafvala A, Shayegh MR, Mazloumi M, Zanganeh S, Lak A, Mohajerani MS, et al. Nanostructure sword-like ZnO wires: rapid synthesis and characterization through a microwave-assisted route. J Alloys Compd. 2009;469:293–7.
84. Bigdeli F, Morsali A, Retailleau P. Syntheses and characterization of different zinc (II) oxide nano-structures from direct thermal decomposition of 1D coordination polymers. Polyhedron. 2010;29:801–6.
85. Patterso A. The Scherrer formula for I-ray particle size determination. J Phys Rev. 1939;56:978–82.
86. Akhtar N, Ihsan-ul-Haq MB. Phytochemical analysis and comprehensive evaluation of antimicrobial and antioxidant properties of 61 medicinal plant species. Arab J Chem. 2018;11:1223–35.
87. Singleton VL, Orthofer R, Lamuela-Raventós RM. Analysis of total phenols and other oxidation substrates and antioxidants by means of Folin-Ciocalteu reagent. Amsterdam: Methods Enzymol. Elsevier; 1999. p. 152–78.
88. Nagajyothi PC, Cha SJ, Yang IJ, Sreekanth TVM, Kim KJ, Shin HM. Antioxidant and anti-inflammatory activities of zinc oxide nanoparticles synthesized using *Polygala tenuifolia* root extract. J Photochem Photobiol B. 2015;146:10–7.
89. Rajakumar G, Thiruvengadam M, Mydhili G, Gomathi T, Chung IM. Green approach for synthesis of zinc oxide nanoparticles from *Andrographis paniculata* leaf extract and evaluation of their antioxidant, anti-diabetic, and anti-inflammatory activities. Bioprocess Biosyst Eng. 2018;41:21–30.
90. Safawo T, Sandeep BV, Pola S, Tadesse A. Synthesis and characterization of zinc oxide nanoparticles using tuber extract of anchote (*Coccinia abyssinica* (Lam.) Cong.) for antimicrobial and antioxidant activity assessment. OpenNano. 2018;3:56–63.
91. Wu TH, Yen FL, Lin LT, Tsai TR, Lin CC, Cham TM. Preparation, physicochemical characterization, and antioxidant effects of quercetin nanoparticles. Int J Pharm. 2008;346:160–8.
92. Khan ZUH, Sadiq HM, Shah NS, Khan AU, Muhammad N, Hassan SU, et al. Greener synthesis of zinc oxide nanoparticles using *Trianthema portulacastrum* extract and evaluation of its photocatalytic and biological applications. J Photochem Photobiol B. 2019;192:147–57.
93. Ahmad I, Alshahrani MY, Wahab S, Al-Harbi AI, Nisar N, Alraey Y, et al. Zinc oxide nanoparticle: an effective antibacterial agent against pathogenic bacterial isolates. J King Saud Univ-Sci. 2022;34:102110.
94. Shinde SS. Antimicrobial activity of ZnO nanoparticles against pathogenic bacteria and fungi. Sci Med Central. 2015;3:1033.
95. Xie Y, He Y, Irwin PL, Jin T, Shi X. Antibacterial activity and mechanism of action of zinc oxide nanoparticles against campylobacter jejuni. Appl Environ Microbiol. 2011;77:2325–31.
96. Huang Z, Zheng X, Yan D, Yin G, Liao X, Kang Y, et al. Toxicological effect of ZnO nanoparticles based on bacteria. Langmuir. 2008;24:4140–4.
97. Bala N, Saha S, Chakraborty M, Maiti M, Das S, Basu R, et al. Green synthesis of zinc oxide nanoparticles using *Hibiscus subdariffa* leaf extract: effect of temperature on synthesis, anti-bacterial activity and anti-diabetic activity. RSC Adv. 2015;5:4993–5003.
98. Bhuyan T, Mishra K, Khanuja M, Prasad R, Varma A. Biosynthesis of zinc oxide nanoparticles from *Azadirachta indica* for antibacterial and photocatalytic applications. Mater Sci Semicond Process. 2015;32:55–61.
99. Agarwal H, Menon S, Kumar SV, Rajeshkumar S. Mechanistic study on antibacterial action of zinc oxide nanoparticles synthesized using green route. Chem Biol Interact. 2018;286:60–70.
100. Nair S, Sasidharan A, Divya Rani VV, Menon D, Nair S, Manzoor K, et al. Role of size scale of ZnO nanoparticles and microparticles on toxicity toward bacteria and osteoblast cancer cells. J Mater Sci Mater Med. 2009;20:235–41.
101. Jayaseelan C, Rahuman AA, Kirthi AV, Marimuthu S, Santhoshkumar T, Bagavan A, et al. Novel microbial route to synthesize ZnO nanoparticles using *Aeromonas hydrophila* and their activity against pathogenic bacteria and fungi. Spectrochim Acta A Mol Biomol Spectrosc. 2012;90:78–84.
102. Mandal AK, Katuwal S, Tettey F, Gupta A, Bhattarai S, Jaisi S, et al. Current research on zinc oxide nanoparticles: synthesis, characterization, and biomedical applications. Nanomaterials. 2022;12:3066.
103. Murali M, Kalegowda N, Gowtham HG, Ansari MA, Alomary MN, Alghamdi S, et al. Plant-mediated zinc oxide nanoparticles: advances in the new millennium towards understanding their therapeutic role in biomedical applications. Pharmaceutics. 2021;13:1662.
104. Mohd Yusof H, Mohamad R, Zaidan UH, Abdul Rahman NA. Microbial synthesis of zinc oxide nanoparticles and their potential application as an antimicrobial agent and a feed supplement in animal industry: a review. J Anim Sci Biotechnol. 2019. https://doi.org/10.1186/s40104-019-0368-z.
105. Elad Y, Yunis H, Katan T. Multiple fungicide resistance to benzimidazoles, dicarboximides and diethofencarb in field isolates of Botrytis cinerea in Israel. Plant Pathol. 1992;41:41–6.
106. Roy Choudhury S, Ghosh M, Mandal A, Chakravorty D, Pal M, Pradhan S, et al. Surface-modified sulfur nanoparticles: an effective antifungal agent against *Aspergillus niger* and Fusarium oxysporum. Appl Microbiol Biotechnol. 2011;90:733–43.
107. Ferrero-Miliani L, Nielsen OH, Andersen PS, Girardin S. Chronic inflammation: importance of NOD2 and NALP3 in interleukin-1β generation. Clin Exp Immunol. 2007;147:227–35.
108. Drozdova IL, Bubenchikov RA. Composition and anti-inflammatory activity of polysaccharide complexes extracted from sweet violet and low mallow. Pharm Chem J. 2005;39:197–200.
109. Mounnissamy VM, Kavimani S, Balu V, Quine SD. Evaluation of anti-inflammatory and membrane stabilizing properties of ethanol extract of *Cansjera rheedii* J. Gmelin (Opiliaceae). IJPT. 2007;6:235–7.

110. Ferrali M, Signorini C, Ciccoli L, Comporti M. Iron release and membrane damage in erythrocytes exposed to oxidizing agents, phenylhydrazine, divicine and isouramil. Biochem J. 1992;285:295–301.
111. Xia T, Kovochich M, Brant J, Hotze M, Sempf J, Oberley T, et al. Comparison of the abilities of ambient and manufactured nanoparticles to induce cellular toxicity according to an oxidative stress paradigm. Nano Lett. 2006;6:1794–807.
112. Selim YA, Azb MA, Ragab I, Abd El-Azim HMM. Green synthesis of zinc oxide nanoparticles using aqueous extract of *Deverra tortuosa* and their cytotoxic activities. Sci Rep. 2020;10:3445.
113. Hassan HFH, Mansour AM, Abo-Youssef AMH, Elsadek BEM, Messiha BAS. Zinc oxide nanoparticles as a novel anticancer approach; in vitro and in vivo evidence. Clin Exp Pharmacol Physiol. 2017;44:235–43.
114. Senthilkumar N, Nandhakumar E, Priya P, Soni D, Vimalan M, Vetha PI. Synthesis of ZnO nanoparticles using leaf extract of: tectona grandis (L.) and their anti-bacterial, anti-arthritic, anti-oxidant and in vitro cytotoxicity activities. New J Chem. 2017;41:10347–56.
115. Manosroi J, Dhumtanom P, Manosroi A. Anti-proliferative activity of essential oil extracted from thai medicinal plants on KB and P388 cell lines. Cancer Lett. 2006;235:114–20.
116. Sana SS, Kumbhakar DV, Pasha A, Pawar SC, Grace AN, Singh RP, et al. Crotalaria verrucosa leaf extract mediated synthesis of zinc oxide nanoparticles: assessment of antimicrobial and anticancer activity. Molecules. 2020;25:4896.
117. Gao Y, Xu D, Ren D, Zeng K, Wu X. Green synthesis of zinc oxide nanoparticles using *Citrus sinensis* peel extract and application to strawberry preservation: a comparison study. Lwt. 2020;126:109297.
118. Umar H, Kavaz D, Rizaner N. Biosynthesis of zinc oxide nanoparticles using *Albizia lebbeck* stem bark, and evaluation of its antimicrobial, antioxidant, and cytotoxic activities on human breast cancer cell lines. Int J Nanomed. 2019;14:87.

Publisher's Note